Review on optofluidic microreactors for photocatalysis

Lei Wang,[1] Ziyu Huang,[1] Xiaohui Yang,[1] Lukas Rogée,[2] Xiaowen Huang,[1*] Xuming Zhang,[2] Shu Ping Lau[2]

[1]Department of Bioengineering; State Key Laboratory of Biobased Material and Green Papermaking; School of Food Science and Engineering; Qilu University of Technology (Shandong Academy of Sciences), Jinan 250353 (China)

[2] Department of Applied Physics, The Hong Kong Polytechnic University, Hong Kong, P.R. China.

*Corresponding author. E-mail: huangxiaowen2013@gmail.com.

Number of words: 9134.

Abstract

Four interrelated issues have been arising with the development of modern industry, namely environmental pollution, the energy crisis, the greenhouse effect and the global food crisis. Photocatalysis is one of the most promising methods to solve them in the future. To promote a high photocatalytic reaction efficiency and utilize solar energy to its fullest, a well-designed photoreactor is vital. Photocatalytic optofluidic microreactors, a promising technology that brings the merits of microfluidics to photocatalysis, offer the advantages of a large surface-to-volume ratio, a short molecular diffusion length and high reaction efficiency, providing a potential method for mitigating the aforementioned crises in the future. Although various photocatalytic optofluidic microreactors have been reported, a comprehensive review of microreactors applied to these four fields is still lacking. In this paper, we review the typical design and development of photocatalytic microreactors in the fields of water purification, water splitting, CO_2 fixation and coenzyme regeneration in the past few years. As the most promising tool for solar energy utilization, we believe that the increasing innovation of photocatalytic optofluidic microreactors will drive rapid development of related fields in the future.

1. Introduction

The development of modern industry has brought with it four interrelated issues, which are water pollution, the energy crisis, the greenhouse effect, and the global food shortage (Hisatomi et al. 2014; Jayamohan et al. 2015; Liu et al. 2014). The wastewater discharge from industrial activities creates severe water pollution, which

leads to public health problems and the degradation of aquatic ecosystems. Meanwhile, the consumption of large amounts of fossil fuels (non-renewable energy), such as coal, oil, and gas, has resulted in the energy crisis, and the scale of this problem is ever increasing. Unfortunately, burning these fossil fuels has also released large amounts of greenhouse gases, leading to global warming, climate change, and glacier melting, thereby seriously damaging the ecological balance and diversity of species (Dodman 2009; Davis and Caldeira 2010). Moreover, the greenhouse effect-induced climate change hinders the growth of crops and thus decreases food production, making the amount of food hardly enough to satisfy the increasing population, intensifying the globally emerging food crisis (Godfray et al. 2010).

Photocatalysis is a photoreaction in the presence of catalysts (generally semiconductor materials) and energy source(UV-Vis light or total solar spectrum), containing both photoinduced oxidation and reduction reactions induced by photo-excited electrons and holes on the surface of the semiconductor catalysts, respectively (Lei et al. 2010). Corresponding to the mentioned four issues, four promising photocatalytic solutions have been proposed and developed (photocatalytic water purification, water splitting, CO_2 fixation, and coenzyme regeneration), which have become prominent research hotspots in recent years (Chen et al. 2015; Coyle and Oelgemöller 2008; Elvira et al. 2013; Erickson et al. 2011; Gemoets et al. 2016; Ji et al. 2016; Kim et al. 2015; Lee et al. 2013; Li et al. 2013; Lin et al. 2011; Ma et al. 2016; Oelgemöller and Shvydkiv 2011; Psaltis et al. 2006; Shvydkiv et al. 2011; Simms et al. 2009; Su and Vayssieres 2016; Whipple et al. 2010; Zhao et al. 2016). Although most of the researches used xenon lamps or LED lamps as light sources, in future practical applications, photocatalytic technology aims to be driven by solar energy. Photocatalytic water purification has the potential to use solar energy and photocatalyst to achieve commercial scale degradation of pollutants in the future. Compared with traditional sewage purification methods (such as electrochemical degradation), photocatalytic water purification has the advantages of environmental protection, energy-saving, and low operating costs due to the use of solar energy and low equipment requirements (Lee and Park, 2013). Photocatalytic water splitting aims

to split water into oxygen and hydrogen， because hydrogen is not only a clean and renewable alternative to fossil energy, but also a raw material for industrial production, such as methanol synthesis, metallurgy, etc. (Chen et al. 2017; Gupta 2017; Midilli et al. 2005; Wang et al. 2019). Except reducing the use of fossil energy, carbon dioxide fixation is another potential strategy to mitigate the greenhouse effect. In nature, carbon dioxide is fixed and converted into carbon compounds in chloroplast matrices through the photosynthesis of green plants (Gust et al. 2009; Lin et al. 2017). By mimicking natural photosynthetic system， synthesis of organic compounds through carbon dioxide fixation is promising strategy that solve the greenhouse effect and food crisis. Thus, the artificial photosynthetic systems have attracted many scholars to research (Cheng et al. 2016; Chen et al. 2017; Kalamaras et al. 2017, 2019; Ryu et al. 2011; Y. Wang et al. 2019; Zhu et al. 2019). For the synthesis of food, such as sugar, the regeneration of nicotinamide adenine dinucleotide hydride/nicotinamide adenine dinucleotide phosphate (NADH/NADPH), which is an essential coenzyme for cellular metabolism and compound synthesis, is a crucial step. With the development of photocatalytic NADH regeneration technology, it is possible to realize the regeneration of NADH effectively in vitro, providing the possibility of artificial-photosynthesis-based food synthesis (Huang et al. 2017; Miller et al. 2020; S. H. Lee et al. 2011; Su et al. 2013; Schwander et al. 2016; Zhao et al. 2019).

Factors such as light irradiation, surface-to-volume ratio (the surface refers to the contact area between the photocatalyst and the reaction liquid, while volume is the amount of reaction liquid in the chamber), and molecular diffusion length are essential elements that impact the photocatalysis efficiency. Thus, reactor designs play a crucial role in photocatalytic efficiency. Well-designed photoreactors can not only promote solar utilization but also improve the reaction rate. Compared with the traditional photocatalytic macroreactors, photocatalytic optofluidic microreactors with immobilized photocatalyst for heterogeneous photocatalysis (reactants and the photocatalysts in different phases) bring the merits of microfluidics to photocatalysis, offering the advantages of large surface-to-volume ratios, short molecular diffusion lengths, and uniform irradiation, which make the photocatalytic optofluidic

microreactors an efficient and promising platform. In the past few years, various optofluidic reactors have been reported in the fields of water purification, water splitting, CO_2 fixation, and coenzyme regeneration, which are expected to improve their photocatalytic efficiency (as shown in Table 1). In this review, we begin with a brief introduction on the mechanism of photocatalysis. Then we will compare traditional photocatalytic macroreactors and photocatalytic optofluidic microreactors, pointing out the major problems of current photocatalytic reactors and the main advantages of photocatalytic optofluidic microreactors. Next, we introduce the latest development of photocatalytic optofluidic microreactors in the fields of water purification, water splitting, CO_2 fixation, and coenzyme regeneration, respectively. Finally, we discuss and look forward to the development direction of photocatalytic optofluidic microreactors in the future.

2. The mechanisms of photocatalysis

Photocatalysis is the acceleration of a chemical reaction in the presence of a catalyst (Shafiq et al., 2021). As soon as the semiconductor photocatalysts are exposed to suitable light, they absorb light energy to drive electron migration. When the energy absorbed by the photocatalyst is greater than or equal to the band gap, electrons of valence band cross the band gap and enter the conduction band with higher energy. The transfer of electron excites an electron in the conduction band and leaves a hole in the valence band, which is referred to as a photogenerated electron-hole pair (Huang et al. 2018; Lee et al. 2013). This photo-generated electron-hole pair will be directly or indirectly involved in the photocatalytic reaction.

In the process of photocatalytic water purification, photo-generated electrons and holes react with water, dissolved oxygen (O_2), hydrogen ions (H^+) as well as hydroxide ions (OH^-) to produce some strongly oxidizing free radicals for the degradation of organic pollutants (as shown in Fig. 1A). Common free radicals are hydroxyl free radicals ($\cdot OH$) and superoxide free radicals ($O_2^{\cdot -}$). (Houas et al. 2001; Tao et al. 2019). Furthermore, holes can also directly participate in the degradation of organic pollutants. During photocatalytic water splitting, the photo-generated hole and

electron pairs react with water, producing oxygen and hydrogen, respectively (Fig. 1B). Regarding the CO_2 fixation, the electrons react with CO_2 adsorbed on the surface of the photocatalyst to reduce it to an organic compound, while the holes react with water to produce H^+, which plays into the CO_2 reduction process (Fig. 1C, take methanol as an example) (Parmar et al. 2015; Ulmer et al. 2019). In the process of the coenzyme regeneration, photo-generated electrons are transferred by electron mediators (M) to NAD^+ and H^+ to regenerate NADH (Fig. 1D). In order to avoid the recombination of photo-generated holes and electrons, these holes are preferably consumed by a sacrifice agent, such as triethanolamine (TEOA) (Yang et al. 2019).

We have reviewed some band gap of photocatalysts and the redox potential of different chemical species in Fig. 2 (Ola and Maroto-Valer, 2015). Taking titanium dioxide (TiO_2) as an example, when the energy of the photon (hν) absorbed by TiO_2 is greater than or equal to the band gap ($h\nu \geqslant 3.2$ eV), the reaction formulas are as follows:

$$TiO_2 + h\nu \rightarrow e_{CB}^- + h_{VB}^+ \quad (1)$$

$$O_2 + e_{CB}^- \rightarrow O_2^{\cdot -} \quad (2)$$

$$(H_2O \leftrightarrow H^+ + OH^-) + h_{VB}^+ \rightarrow \cdot OH + H^+ \quad (3)$$

$$O_2^{\cdot -} + H^+ \rightarrow HO_2^{\cdot} \quad (4)$$

$$2\ HO_2^{\cdot} \rightarrow H_2O_2 + O_2 \quad (5)$$

$$H_2O_2 + e_{CB}^- \rightarrow \cdot OH + OH^- \quad (6)$$

$$Pol + \cdot OH/O_2^{\cdot -}/h_{VB}^+ \rightarrow \text{Degradation products} \quad (7)$$

$$2\ H_2O + 4\ h_{VB}^+ \rightarrow 4H^+ + O_2 \quad (8)$$

$$2\ H^+ + 2\ e_{CB}^- \rightarrow H_2 \quad (9)$$

$$CO_2 + 6\ H^+ + 6\ e_{CB}^- \rightarrow CH_3OH + H_2O \quad (10)$$

$$NAD^+ + H^+ + 2\ e_{CB}^- \rightarrow NADH \quad (11)$$

Equation 1 represents the process of the photocatalyst absorbing photons to

generate electron(e_{CB}^-)-hole(h_{VB}^+) pairs; equations 2-6 represent the formation process of $O_2^{\cdot -}$ and ·OH; equations 7 is the degradation process of organic pollutants, where "Pol" represent pollutants; equation 8 and equation 9 respectively illustrates the generation process of oxygen and hydrogen in the photocatalytic water splitting process; equations 10 represents the process of CO_2 reduction to generate methanol; equation 11 shows the regeneration process of NADH, NAD^+ and H^+ in the solution accept photo-generated electrons from the photocatalyst to regenerate NADH.

3. Comparison of traditional photocatalytic macroreactor and photocatalysis optofluidic microreactor

The design of photocatalytic reactors plays a crucial role in efficiency, leading to numerous innovative reactor designs, which can be divided into traditional photocatalytic macroreactors and photocatalysis optofluidic microreactors according to the volumetric capacity generated from the dimensions of the channels (Mehendafe, Jacobi and Shah, 2000). The hydraulic diameter (D_h) of the channel in traditional photocatalytic macroreactor usually is larger than 1 mm, while that of photocatalysis optofluidic microreactor is less than 1 mm (De Sá et al. 2016; Mehendale, Jacobi and Shah 1999). Furthermore, depending on the phase of catalyst and reactants, traditional photocatalytic macroreactors can be divided into two types, namely homogeneous macroreactors (reactants and the photocatalysts in the same phase) and heterogeneous macroreactors (reactants and the photocatalysts in different phases) (Cieśla et al. 2004; Augugliaro et al. 2006; Parrino and Palmisano 2021; Behnajady et al. 2007; Cassano et al. 1995; Jin et al. 2005; Ku et al. 2001; Lee et al. 2002; Liou et al. 2011; McCullagh et al. 2011; Nguyen and Wu 2008; Wang and Ku 2003; Wu et al. 2005; Wu et al. 2008; Yuan et al. 2014). Homogeneous macroreactors, as shown in Fig 3A and 3B, are divided into batch macroreactors and flow mode macroreactors. The volume of batch macroreactors generally ranges from several cubic centimeters to hundreds of cubic centimeters, while the D_h of flow mode macroreactors is usually larger than 1 mm (De Sá et al. 2016; Wu et al. 2015). They are both simple in construction, low cost and have the potential to be designed as industrial reactors with

larger volumes (Lu et al. 2014). However, in the homogeneous macroreactors, the suspended photocatalyst and molecular diffusion length (millimeters or centimeters) lead to uneven irradiation and poor mass transfer efficiency, respectively, unfortunately resulting in the low photon utilization and low catalytic efficiency. (Leblebici et al. 2015; Potti and Srivastava 2012; Tsuchiya et al. 2012; Priyanka and Srivastava 2013). Furthermore, the photocatalyst is dispersed in the reaction solution, which requires certain specific steps to recover the catalyst. Wall-coated macroreactor (Fig. 3C) is a type of heterogeneous macroreactors in which the catalyst is coated on the inner wall of the reactor without any complex catalyst recovery steps unnecessary. Unfortunately, the surface-to-volume ratio of the wall-coated photoreactors is small (usually < 400 $m^2 \cdot m^{-3}$), resulting in poor catalytic efficiency (Van Gerven et al. 2007). Thus, the honeycomb optical fiber macroreactors were designed (Fig. 3D). In this type, parallel channels and immobilized catalysts increase the surface-to-volume ratio to 1000-2000 $m^2 \cdot m^{-3}$ and improve the catalytic efficiency of the reactor (Denny et al. 2010; Van Gerven et al. 2007; Wang et al. 2010). Meanwhile, the multi-channel design significantly enhances the reaction throughput. However, honeycomb fiber macroreactors have a low utilization rate of photons due to its opaqueness. In Table 2, we summarize the main macroreactors used for photocatalysis. For the author's convenience to compare of photocatalytic efficiency in different reactors, uniform parameters are important to be introduced. Thus, we suggest uniform parameters, such as the space time yield (STY) or the photocatalytic space time yield (PSTY), quantum yield and electrical energy per order (EEO), which are significant for the improvement and development of the photocatalysis reactors.

Microfluidics have many merits in the field of photocatalysis, such as controllable microstructures, precise manipulation of small volumes of fluids, fine flow control, large surface-to-volume ratio, short molecular diffusion length, and uniform irradiation. Photocatalytic optofluidic microreactors ($D_h < 1$ mm) combine the advantages of heterogeneous photocatalysis and microfluidic ((De Sá et al., 2016), Gust et al. 2009; Han et al. 2013; Jayamohan et al. 2016), having the potential to effectively solve the drawbacks of traditional photocatalytic macroreactors (Gorkin et

al. 2010; Whitesides 2006; Wang et al. 2012, 2014; Zhao et al. 2014). Based on the reported works, photocatalytic optofluidic microreactors can be mainly classified into four types depending on the material and structure, namely capillary tube microreactors (Fig. 3E), single-microchannel reactors (Fig. 3F), multi-microchannel reactors (Fig. 3G), and planar microreactors (Fig. 3H). The advantages of these photocatalytic optofluidic microreactors are as follows: First, the larger surface-to-volume ratio (10000-300000 m^2 m^{-3}) effectively increases the contact area between the catalyst and the reactant, thus improving the catalytic efficiency (Elvira et al. 2013; Van Gerven et al. 2007). It is noted that in a microreactor with columnar chamber the value of the surface-to-volume ratio is equal to 1/h (where the h is the height of the chamber). In fact, the real value of the surface-to-volume ratio is much larger than 1/h due to the nanopores of the photocatalyst (Wang et al. 2014). Second, the advantage of the small size allows only a thin layer of liquid (<1 mm) to flow on the immobilized photocatalyst, which is conducive to uniform illumination, andensuring a high photon efficiency. The reason is that the reaction rate is proportional to the radiant flux Φ (Φ≤25 mW/cm^2) or the square root of radiant flux (Φ＞25 mW/cm^2) (Herrmann, J. M. 1999). Third, different from traditional optical fiber reactors, photocatalytic optofluidic microreactors are usually made of transparent materials, which significantly improve the photon utilization rate. Fourth, microreactors require less photocatalyst material, thus decreasing the cost (Azzouz et al. 2018). Fifth, the molecular diffusion length of photocatalytic optofluidic microreactors is on the micron scale, which allows the reactant diffusion to the reaction surface faster (Wang et al. 2014). Sixth, optofluidic reactors have extended functions on the basis, such as on-chip monitoring, on-chip assembling with external magnetic/electric/sound/heating fields, parallel processing for rapid screening of photocatalysts, etc. (Accardo et al. 2013; Collin et al. 2016; Fan and White 2011; Fan and Yun 2014; Huang et al. 2014; Huang, Yue et al. 2016; Li et al. 2016; Sun and Fang 2010; Wang et al. 2012; Zhang et al. 2013). In table 3, we summarized the main comparation of traditional photocatalytic macroreactors and photocatalytic optofluidic microreactors.

4. Water purification

In recent years, microreactor-based photocatalytic water purification has been continuously optimized in terms of catalytic efficiency with the constant innovation of microreactors designs. Nagamine (2020) designed a novel photocatalysis optofluidic microreactor utilizing the charge separation effect of TiO_2/Ti plates, as shown in Fig. 4A. The hole and electron pairs of TiO_2 were separated via TiO_2/Ti plates on which the oxidation and reduction were conducted in different microchannels. Azzouz et al. (2018) designed a zinc oxide nanometer photocatalytic optofluidic microreactors, in which the zinc oxide nanowires (ZnO NWs) were fixed on the silicon substrate of the reactor through an in-situ growth method. To increase the specific surface area and mass transfer rate, a microcolumn array was introduced into the reaction chamber, inside which the methylene blue (MB) degradation rate reached 95 % with initial concentration of 2000 μg mL^{-1} within 5 s of residence time. The standard catalytic efficiency was calculated to be 2.28×10^4 μg mL^{-1} min^{-1}, which is typically 5 orders of magnitude larger than that of macroreactors. Zhang et al. (2020) reported a capillary microreactor packed with TiO_2-coated glass beads to increase the supporting area of the catalyst and shorten the mass transfer route, as shown in Fig. 4B. As a result, the corresponding degradation rate of MB was close to 100 % with the initial concentration of 3.13×10^{-5} mol L^{-1} under 20 s of irradiation, converting to ~28.83 μg mL^{-1} min^{-1} as a standard catalytic efficiency. Furthermore, the microreactor had good durability, with a decline of only about 10 % after six hours of operation. Recently, studies on the gas-liquid-solid microreactor aroused the interest of scientists. Chen et al. (2018) conducted a visualization study on the interaction between Taylor flow behavior and catalytic activity in a long-running gas-liquid-solid microreactor, which provided a basis for the development of gas-liquid-solid photocatalysis optofluidic microreactor. Yu and Wang (2020) reported a gas-liquid-solid three-phase photocatalysis optofluidic microreactor with two parts: a beaked bubble generator and a helical microchannel reaction chamber (Fig. 4C). Inside the channel, TiO_2 was immobilized in situ by dopamine in the reaction chamber (the yellow part), and the

addition of gas helped to remove the water film attracting to the photocatalyst surface, which results in enhanced mass transfer and self-refreshment. Moreover, experimental data showed that oxygen bubbles could provide sufficient oxygen for photocatalysis and photodegradation. The results show that it not only reduces the number of hole-electron combinations, but also improves the degradation efficiency of MB.

Besides the inner structure of photocatalytic optofluidic microreactors, the performance of photocatalyst is another determinant of the photocatalytic efficiency in microreactors, such as the morphology and light absorption, (Ola and Maroto-Valer, 2015). Specifically, Nagamine and Inohara (2018) used anodized TiO_2 nanotubes/Ti bi-layer plates to prepare a photocatalytic optofluidic microreactor, in which the length and inner diameter of TiO_2 werecontrolled by anodization voltage and time. They found that the photocatalytic activity of TiO_2 nanotubes increased with the increase in length and inner diameter. Furthermore, the plasmonic nanoparticles doping of photocatalytic materials is a good way to increase the performance of photocatalyst. The strong field enhancement caused by plasmonic nanoparticles (e.g., Au, Ag, Al, CuO) increases the absorption cross-section of the semiconductor, resulting in the extension of light absorption to longer wavelengths and enhancing the electron-hole charge separation in the semiconductor medium, thereby maximizing the photocatalytic efficiency (Adleman et al., 2009; Christopher, Xin and Linic, 2011; Linic, Christopher and Ingram, 2011; Zhou et al., 2015). Jia et al. (2019) designed a microreactor with a TiO_2 membrane modified with gold nanoparticles (Au NPs), which significantly improved the photocatalytic efficiency (Fig. 5). The rough surface of TiO_2/AuNP on FTO increased the surface area, and the AuNPs helped to achieve strong absorption of visible light. Compared with pure TiO_2 membrane microreactors, TiO_2/AuNP membrane microreactors increased the reaction rate for MB degradation by a factor of 13. Except for Au NPs, combining photocatalysts with other metal materials also improves photocatalytic efficiency by enhancing the separation of charge holes. Martin et al. (2019) reported a photocatalytic optofluidic microreactors containing cerium-doped TiO_2 films, showing that different concentrations of cerium affect both light absorption and degradation. The highest absorption efficiency of the

film was 0.8 nominal atomic % of cerium (0.8 Ce at. %), while the maximum degradation efficiency of Ce was 0.3 Ce at. % (0.55 μg mL^{-1} min^{-1}). The reason was the right concentration of Ce^{3+}/Ce^{4+} pairs acting as an electron scavenger to prevent the recombination of holes and electrons. Nonetheless, an excess of Ce^{3+}/Ce^{4+} pairs would act as the recombination centers, decreasing the photocatalytic activity.

5. Water splitting

Photocatalytic optofluidic microreactors were reported to significantly improve the catalytic efficiency of water splitting (Chen et al. 2017; Sarkar and Bhattacharyya 2012). Ahsan et al. (2013) proposed a pioneering study on photocatalytic water splitting using microfluidic platforms. The reaction rate and efficiency had at least 2-fold improvement by simply increasing flow rate. Recently, new achievements using photocatalytic optofluidic microreactors in water splitting came about (Fajrina and Tahir 2019; Jafari et al. 2016), such as novel microreactors of polyacrylamide (PAM)-CdS microgels in which the H_2 production rate was up to 5.21 mmol g_{cat}^{-1} h^{-1}. The PAM microgel used for the immobilized substrate of photocatalyst nano CdS prevented photocatalyst aggregation. The N-Cd bond and electrostatic interaction respectively promote the transfer of electrons from PAM to CdS and hinder the recombination of electron-hole pairs, both of which result in more electrons participating in the H_2 production process (An et al. 2019). Traditional photocatalytic optofluidic microreactors with the planar design have a small active surface area and low mass transport rate, which limiting photocatalytic efficiency. The photocatalytic optofluidic microreactors with staggered micro-pillars in the reaction microchamber designed by Li et al. (2014) effectively solve these problems. As shown in Fig. 6A, the introduction of staggered micro-pillars increased the active surface area. Itenhanced the mass transfer efficiency, which resulted in a 56% increase in catalytic efficiency compared with planar reactors. Besides liquid-phase reaction, gas-phase photocatalytic H_2 generation was developed. Castedo et al. (2018) using a small microreactor to study the effect of temperature on the photocatalytic hydrogen production in the gas phase (Fig. 6B). In their experiment, the generation of hydrogen

followed the Langmuir-Hinshelwood model under UVA irradiation. Under different irradiances, the generation of hydrogen is favored by the increase of temperature following the Arrhenius relation. The amount of H_2 produced reached 0.99 ± 0.024 mmol g_{cat}^{-1} h^{-1} at 348 K (room temperature) and 1.5 mW·cm^{-2} (illumination intensity). Furthermore, they found that the microreactor scaled up by a factor of ~10 produces a very similar result, which demonstrated the feasibility of the amplification technology to achieve solar hydrogen production. Most of the current studies mainly focused on the hydrogen-producing part. Oxygen generation is another important part of photocatalytic water splitting. Photocatalysts, such as $SrTiO_3$, $KTaO_3$, $In_2O_3(ZnO)_3$, $SrTiO_3$:Cr/Sb were developed for overall water splitting (Kudo and Miseki 2009). Q. Wang et al. (2019) prepared a Cr_2O_3/Rh/IrO_2-modified $Y_2Ti_2O_5S_2$ photocatalyst with improved activation and stabilization, achieving simultaneous production of stoichiometric amounts of hydrogen and oxygen on $Y_2Ti_2O_5S_2$ during a 20 h reaction.

6. CO_2 fixation

The application of photocatalytic optofluidic microreactors in the field of photocatalytic CO_2 fixation effectively improves the conversion efficiency (Cheng et al. 2017; Ma et al. 2014; Qin et al. 2011; Zeng et al. 2014). Chen et al. (2017) designed a photocatalysis optofluidic microreactor with a membrane for photocatalytic CO_2 reduction. As shown in Fig. 7A, this mesoporous CdS/TiO_2/SBA-15@carbon paper composite membrane used as photocatalyst has a high surface-to-volume ratio and pore volume, beneficial for studying the effects of liquid flow rate, light intensity, and NaOH concentration on the conversion efficiency. Under the optimal conditions, the maximum methanol production rate reaches 1.022 mmol g_{cat}^{-1} h^{-1}, which is nearly 4 times higher than for CdS/TiO_2. However, the product of the photocatalytic CO_2 reduction had poor selectivity, which limits its application range. For the problem, Xie et al. (2019) designed a coupled system that integrated photocatalytic reduction of CO_2 with photocatalytic fuel cells (PFC). As shown in Fig. 7B, the product obtained by the photocatalytic reduction of CO_2 was directly used as the fuel of PFC to generate electricity. With CO_2, the current density

and maximum output power were significantly increased. The fuel concentration at the PFC export was even higher than that at the PFC import, indicating the feasibility of the coupling system for power generation and solar fuel. Another couple system, the photosynthetic hybrid system, which is the combination of photocatalysts and microbial systems. It cooperates with the good light absorption performance of solid photocatalyst and good biocatalyst performance to achieving the selective conversion of CO_2. Sakimoto et al. (2016) integrated a self-augmented biological system, a non-photosynthetic bacterium with CdS nanoparticles (photocatalysts), enabling the selective photosynthesis of acetic acid from CO_2 for several days, and working as a novel CO_2 reduction microreactor. Then, to avoid the toxicity of CdS, Zhang et al. (2018) reported a gold nanocluster (AuNCs) based biocompatible photocatalyst, which significantly increased the efficiency of acetic acid generation (Fig. 8A and 8B). In detail, AuNCs function as a reactive oxygen scavenging agent and increase the survival rate of *M. thermoacetica*. This system demonstrated a high continuity and consistency capable of converting CO_2 for several days. Besides the semiconductor materials-based bio-hybrid systems, Miller et al. (2020) successfully developed an artificial chloroplast system for CO_2 fixation, made by microfluidic technology to encapsulate the thylakoid membrane of spinach in cell- sized droplets, which was energized by light to power enzymes or enzyme cascades (Fig. 8C and 8D). After that, the droplets were combined with the Crotonyl–coenzyme A (CoA)/ethylmalonyl CoA/hydroxybutyryl CoA (CETCH) cycle to convert CO_2 to glycolate (Fig. 8E). Although the overall productivity of the complex system was lower than that of a single Crotonyl-coenzyme A (CoA) carboxylase/reductase (Ccr), it was still superior to a single enzyme, showing the possibility of creating new-to-nature photosynthetic entities that have the potential to outcompete natural photosynthesis.

7. Regeneration of coenzyme

In plants, sugar production relies on the Calvin cycle, in which the coenzyme NADPH plays an important role. Thus, the regeneration of $NADP^+$ to NADPH /NAD^+ and then to NADH is crucial. Based on the merits of

microfluidics/optofluidics, various works for coenzyme regeneration were reported. J. S. Lee et al. (2011) proposed a microfluidic method to form an artificial photosynthetic system. As shown in Fig. 9A, this microreactor has two components, the light-dependent zone with a photocatalyst (CdSe) and the light-independent zone with glutamate dehydrogenase (GDH), realizing NADH regeneration and L-glutamate synthesis, respectively. Traditional methods for the fabrication of artificial coenzyme regeneration systems in optofluidic microreactors usually contain three steps, including the immobilization of the photocatalyst, the synthesis of a suitable electron mediator (M), and the introduction of the M into the reaction system. To make this process simpler, Huang, Liu, et al. (2016) designed a one-step method for coenzyme regeneration in photocatalytic optofluidic microreactors (Fig. 9B and 9C). Mixing a pentamethylcyclopentadienylrhodium (III) chloride dimer, 2,2'-bipyridyl and a graphitic carbon nitride photocatalyst (g-C_3N_4) in ethanol and then evaporating the mixture at 50 ℃ resulted in a residue that can function as an immobilized artificial photosystem I (IAPSI) containing the photocatalysts and the M. This one-step method saves time and reduces the chance to obtain impurities to some extent. Moreover, the regeneration efficiency of NADH is 1.12 mmol L^{-1} h^{-1}, which is 2.3 times faster than the homogeneous photocatalytic system. Mimicking cellular structures has also been one of the directions of microreactor design in recent years. Lin et al. (2018) reported an alcohol dehydrogenase(ADH)@nano TiO_2 bioinspired microreactor, in which the ADH was encapsulated by TiO_2 nanoparticles and coupled with the photocatalytic system. In this coupled system, the regenerated NADH was directly supplied to ADH as the useful coenzyme for sustainable biosynthesis under visible light irradiation. However, in photocatalytic-enzyme systems, the catalytic efficiency is still affected by poor electron transfer and oxidative inactivation of the enzyme during the photoreaction process. To solve these problems, some works are reported. Tian et al. (2020) constructed a novel functionally partitioned photocatalyst-enzyme system (TPE-C3N4/PEI/Rh and FDH@MAF-7) inspired by the structure of thylakoid. They synthesized a complete artificial photosystem by conjugation the Rh complex (electron mediator) onto thiophene-modified C_3N_4 (TPE-C_3N_4), using the

polyethylenimine (PEI) as a molecular linker. The tight integration of the photocatalyst and the Rh complex greatly enhanced the electron transfer, allowing the regeneration efficiency of NADH to reach 9.33 μM min^{-1}. Meanwhile, the formate dehydrogenase (FDH) was encapsulated in the metal-organic framework MAF-7, avoiding the effect of reactive oxygen species generated during the photocatalytic process on the enzyme.

8. Discussions and outlook

Photocatalytic optofluidic microreactors effectively overcome the problems of uneven illumination, poor mass transfer, low photon utilization in the traditional homogeneous photoreactors and the low surface-to-volume rate in the traditional heterogeneous photoreactors. The application of photocatalytic optofluidic microreactors in terms of water purification, water splitting, CO_2 fixation, coenzyme regeneration is a promising solution for the environmental pollution, energy crisis, greenhouse effect and global food crisis. However, the current photocatalytic optofluidic microreactors still have certain limitations, such as low throughput. Although the microreactors multi-parallel and the bundle of capillary tubes are effective ways to expand the reaction throughput (de Sá et al. 2018), more microreactors undoubtedly increase its cost. For high throughput and production, a feasible solution is that to scale up the size of the microreactor, while maintaining the original characteristics (high photon utilization, high mass transfer efficiency, high specific surface area, etc.). Therefore, it is a crucial task to study the intrinsic kinetic characteristics of various photocatalytic reactions by combining microreactors with analytical detection technologies such as in-situ surface and bulk spectroscopies (Russo, 2021). According to the basic steps in the photocatalytic process, the rate-limiting step, and the characteristic parameters such as adsorption and desorption, it would be possible to scale up the reactor. Beyond that, based on the modeling of related parameters to infer the catalytic amplified efficiency or other characteristic parameters, which will play a guiding role in the scale-up of the microreactor. In fact, in other application scenarios, the micro-size of the microreactor is an advantage, such

as analysis and detection. The miniaturization of the photocatalytic reaction on the microfluidic chip significantly increases the reaction rate, reduces the consumption of samples and reagents, and increases the throughput of parallel screening of samples (Zhang et al. 2013).

Except the innovative design of the microreactors, optimizing the photocatalyst is another solution. Most of the existing photocatalytic materials are semiconductor materials, such as TiO_2 and g-C_3N_4. Although they have been applied in many fields, there is still some problems One problem is the limited production amount caused by the low stability of the catalyst and the low selectivity of the product in the field of photocatalytic CO_2 fixation and water splitting. Therefore, the preparation of new photocatalysts with high stability and high selectivity is a development trend for improving the catalytic efficiency of related fields (Ola and Maroto-Valer, 2015). Another problem is the high band gap of the semiconductor catalyst limits its absorption of visible light. So photocatalyst modification is also a feasible solution to improve the catalytic efficiency. Doping of plasma and photocatalyst can significantly enhance light absorption, thereby improving photocatalytic efficiency. In the fourth section of this review, we discussed several related works on the modification of other photocatalytic materials. Compared with the degradation of pure photocatalysts, the degradation efficiency of the doped photocatalysts is significantly improved. However, the plasma is mainly precious metal materials such as Au nanoparticles. To reduce costs, improving the stability and recyclability of photocatalysts doped with plasma is a future development trend.

The innovative design of novel microreactor, the expansion of microreactor throughput, and the development and modification of photocatalytic materials are effective ways to efficiently develop and utilize solar energy to realize the commercial production of photocatalytic products. We believe that the exploration of the above challenges will promote the rapid development of photocatalytic optofluidic microreactors and their practical applications.

Conflicts of interest

There are no conflicts to declare.

Acknowledgements

This research was funded by Shandong Provincial Key Research and Development Project (2020CXGC011304); National Natural Science Foundation of China (Grant No. 32001020； No. 82130067); Shandong Provincial Natural Science Foundation (ZR2020QB131); Qilu University of Technology Foundation/Shandong Academy of Sciences Foundation (202004).

References

Accardo, A., Mecarini, F., Leoncini, M., Brandi, F., Di Cola, E., Burghammer, M., Riekel, C. and Di Fabrizio, E. (2013). Fast, active droplet interaction: Coalescence and reactive mixing controlled by electrowetting on a superhydrophobic surface. Lab Chip 13: 332-335.

Adleman, J. R., Boyd, D. A., Goodwin, D. G. and Psaltis, D. (2009). Heterogenous catalysis mediated by plasmon heating. Nano Letters. 9: 4417-4423.

Ahsan, S. S., Gumus, A. and Erickson, D. (2013). Redox mediated photocatalytic water-splitting in optofluidic microreactors. Lab Chip 13: 409-414.

An, Z., Gao, J., Wang, L., Zhao, X., Yao, H., Zhang, M., Tian, Q. and Liu, Y. (2019). Novel microreactors of polyacrylamide (PAM)-CdS microgels for admirable photocatalytic H_2 production under visible light. Int. J. Hydrogen Energy 44: 1514-152.

Azzouz, I., Habba, Y. G., Capochichi-Gnambodoe, M., Marty, F., Vial, J., Leprince-Wang, Y. and Bourouina, T. (2018). Zinc oxide nano-enabled microfluidic reactor for water purification and its applicability to volatile organic compounds. Microsyst. Nanoeng. 4: 1-7.

Behnajady, M. A., Modirshahla, N., Daneshvar, N. and Rabbani, M. (2007). Photocatalytic degradation of an azo dye in a tubular continuous-flow photoreactor with immobilized TiO_2 on glass plates. Chem. Eng. J. 127: 167-176.

Cassano, A. E., Martín, C. A., Brandi, R. J. and Alfano, O. M. (1995). Photoreactor Analysis and Design: Fundamentals and Applications. Ind. Eng. Chem. Res. 34: 2155-2201.

Castedo, A., Casanovas, A., Angurell, I., Soler, L. and Llorca, J. (2018). Effect of temperature on the gas-phase photocatalytic H_2 generation using microreactors under UVA and sunlight irradiation. Fuel 222: 327-333.

Chen, R., Cheng, X., Zhu, X., Liao, Q., An, L., Ye, D., He, X. and Wang, Z. (2017). High-performance optofluidic membrane microreactor with a mesoporous CdS/TiO_2/SBA-15@carbon paper composite membrane for the CO_2 photoreduction. Chem. Eng. J. 316: 911-918.

Chen, R., Feng, H., Zhu, X., Liao, Q., Ye, D., Liu, J., Liu, M., Chen, G. and Wang, K. (2018). Interaction of the Taylor flow behaviors and catalytic reaction inside a gas-liquid-solid microreactor under long-term operation. Chem. Eng. Sci. 175: 175-184.

Chen, R., Li, L., Zhu, X., Wang, H., Liao, Q. and Zhang, M. X. (2015). Highly-durable optofluidic

microreactor for photocatalytic water splitting. Energy 83: 797-804.

Chen, S., Takata, T. and Domen, K. (2017). Particulate photocatalysts for overall water splitting. Nat. Rev. Mater. 2: 1-17.

Chen, Y. L., Kuo, L. C., Tseng, M. L., Chen, H. M., Chen, C. K., Huang, H. J., Liu, R. S. and Tsai, D. P. (2013). ZnO nanorod optical disk photocatalytic reactor for photodegradation of methyl orange. Opt. Express 21: 7240.

Cheng, M., Yang, S., Chen, R., Zhu, X., Liao, Q. and Huang, Y. (2017). Copper-decorated TiO_2 nanorod thin films in optofluidic planar reactors for efficient photocatalytic reduction of CO_2. Int. J. Hydrogen Energy 42: 9722-9732.

Cheng, X., Chen, R., Zhu, X., Liao, Q., He, X., Li, S. and Li, L. (2016). Optofluidic membrane microreactor for photocatalytic reduction of CO_2. Int. J. Hydrog. Energy 41: 2457-2465.

Chong, M. N., Jin, B., Chow, C. W. K. and Saint, C. (2010). Recent developments in photocatalytic water treatment technology: A review. Water Research 44: 2997-3027.

Christopher, P., Xin, H. and Linic, S. (2011). Visible-light-enhanced catalytic oxidation reactions on plasmonic silver nanostructures. Nature Chemistry. 3: 467-472.

Collin, W. R., Scholten, K. W., Fan, X., Paul, D., Kurabayashi, K. and Zellers, E. T. (2016). Polymer-coated micro-optofluidic ring resonator detector for a comprehensive two-dimensional gas chromatographic microsystem: μGC×μGC-μOFRR. Analyst 141: 261-269.

Coyle, E. E. and Oelgemöller, M. (2008). Micro-photochemistry: photochemistry in microstructured reactors. The new photochemistry of the future?. Photochem. Photobiol. Sci. 7: 1313.

Davis, S. J. and Caldeira, K. (2010). Consumption-based accounting of CO_2 emissions. Proc. Natl. Acad. Sci. U. S. A. 107: 5687-5692.

Denny, F., Scott, J., Peng, G. D. and Amal, R. (2010). Channelled optical fibre photoreactor for improved air quality control. Chem. Eng. Sci. 65: 882-889.

Dionysiou, D. D., Khodadoust, A. P., Kern, A. M., Suidan, M. T., Baudin, I. and Laîné, J. M. (2000). Continuous-mode photocatalytic degradation of chlorinated phenols and pesticides in water using a bench-scale TiO_2 rotating disk reactor. Appl. Catal., B 24: 139-155.

Dodman, D. (2009). Blaming cities for climate change? An analysis of urban greenhouse gas emissions inventories. Environment and Urbanization 21: 185-201.

Elvira, K. S., I Solvas, X. C., Wootton, R. C. R. and Demello, A. J. (2013). The past, present and

potential for microfluidic reactor technology in chemical synthesis. Nat. Chem. 5: 905-915.

Erickson, D., Sinton, D. and Psaltis, D. (2011). Optofluidics for energy applications. Nat. Photonics 5: 583-590.

Fajrina, N. and Tahir, M. (2019). A critical review in strategies to improve photocatalytic water splitting towards hydrogen production. Int. J. Hydrogen Energy 44: 540-577.

Fan, X. and White, I. M. (2011). Optofluidic microsystems for chemical and biological analysis. Nat. Photonics 5: 591-597.

Fan, X. and Yun, S. H. (2014). The potential of optofluidic biolasers. Nat. Methods 11: 141-147.

Gemoets, H. P. L., Su, Y., Shang, M., Hessel, V., Luque, R. and Noël, T. (2016). Liquid phase oxidation chemistry in continuous-flow microreactors. Chem. Soc. Rev. 45: 83-117.

Van Gerven, T., Mul, G., Moulijn, J. and Stankiewicz, A. (2007). A review of intensification of photocatalytic processes. Chem. Eng. Process. 46: 781-789.

Godfray, H. C. J., Beddington, J. R., Crute, I. R., Haddad, L., Lawrence, D., Muir, J. F., Pretty, J., Robinson, S., Thomas, S. M. and Toulmin, C. (2010). Food Security: The Challenge of Feeding 9 Billion People. Science 327: 812-818.

Gorkin, R., Park, J., Siegrist, J., Amasia, M., Lee, B. S., Park, J. M., Kim, J., Kim, H., Madou, M. and Cho, Y. K. (2010). Centrifugal microfluidics for biomedical applications. Lab Chip 10: 1758-1773.

Gupta, N. M. (2017). Factors affecting the efficiency of a water splitting photocatalyst: A perspective. Renewable Sustainable Energy Rev. 71: 585-601.

Gust, D., Moore, T. A. and Moore, A. L. (2009). Solar fuels via artificial photosynthesis. Acc. Chem. Res. 42: 1890-1898.

Han, Z., Li, J., He, W., Li, S., Li, Z., Chu, J. and Chen, Y. (2013). A microfluidic device with integrated ZnO nanowires for photodegradation studies of methylene blue under different conditions. Microelectron. Eng. 111: 199-203.

Herrmann, J. M. (1999). Heterogeneous photocatalysis: fundamentals and applications to the removal of various types of aqueous pollutants. Catal. Today. 53: 115-129.

Hisatomi, T., Kubota, J. and Domen, K. (2014). Recent advances in semiconductors for photocatalytic and photoelectrochemical water splitting. Chem. Soc. Rev. 43: 7520-7535.

Houas, A., Lachheb, H., Ksibi, M., Elaloui, E., Guillard, C. and Herrmann, J. M. (2001). Photocatalytic degradation pathway of methylene blue in water. Appl. Catal., B 31: 145-157.

Huang, X., Hao, H., Liu, Y., Zhu, Y. and Zhang, X. (2017). Rapid Screening of Graphitic Carbon Nitrides for Photocatalytic Cofactor Regeneration Using a Drop Reactor. Micromachines 8: 175.

Huang, X., Hui, W., Hao, C., Yue, W., Yang, M., Cui, Y. and Wang, Z. (2014). On-site formation of emulsions by controlled air plugs. Small 10: 758-765.

Huang, X., Liu, J., Yang, Q., Liu, Y., Zhu, Y., Li, T., Tsang, Y. H. and Zhang, X. (2016). Microfluidic chip-based one-step fabrication of an artificial photosystem I for photocatalytic cofactor regeneration. RSC Adv. 6: 101974-101980.

Huang, X., Wang, J., Li, T., Wang, J., Xu, M., Yu, W., Abed, A. El and Zhang, X. (2018). Review on optofluidic microreactors for artificial photosynthesis. Beilstein J. Nanotechnol. 9: 30-41.

Huang, X., Yue, W., Liu, D., Yue, J., Li, J., Sun, D., Yang, M. and Wang, Z. (2016). Monitoring the intracellular calcium response to a dynamic hypertonic environment. Sci. Rep. 6: 1-8.

Jafari, T., Moharreri, E., Amin, A. S., Miao, R., Song, W. and Suib, S. L. (2016). Photocatalytic water splitting-The untamed dream: A review of recent advances. Molecules 21: 900.

Jayamohan, H., Smith, Y. R., Gale, B. K., Mohanty, S. K. and Misra, M. (2016). Photocatalytic microfluidic reactors utilizing titania nanotubes on titanium mesh for degradation of organic and biological contaminants. J. Environ. Chem. Eng. 4: 657-663.

Jayamohan, H., Smith, Y. R., Hansen, L. C., Mohanty, S. K., Gale, B. K. and Misra, M. (2015). Anodized titania nanotube array microfluidic device for photocatalytic application: Experiment and simulation. Appl. Catal., B 174-175: 167-175.

Ji, X., Su, Z., Wang, P., Ma, G. and Zhang, S. (2016). Integration of Artificial Photosynthesis System for Enhanced Electronic Energy-Transfer Efficacy: A Case Study for Solar-Energy Driven Bioconversion of Carbon Dioxide to Methanol. Small 12: 4753-4762.

Jia, H., Wong, Y. L., Jian, A., Tsoi, C. C., Wang, M., Li, W., Zhang, W., Sang, S. and Zhang, X. (2019). Microfluidic Reactors for Plasmonic Photocatalysis Using Gold Nanoparticles. Micromachines 10: 869.

Jin, H. J., Sang, D. K., Tak, H. L. and Dong, H. L. (2005). Degradation of trichloroethylene by photocatalysis in an internally circulating slurry bubble column reactor. Chemosphere 60: 1162-1168.

Kalamaras, E., Belekoukia, M., Tan, J. Z. Y., Xuan, J., Maroto-Valer, M. M. and Andresen, J. M. (2019). A microfluidic photoelectrochemical cell for solar-driven CO_2 conversion into liquid fuels with CuO-based photocathodes. Faraday Discuss. 215: 329-344.

Kalamaras, E., Maroto-Valer, M., Xuan, J. and Wang, H. (2017). A Microfluidic Reactor for Solar Fuel Production from Photocatalytic CO_2 Reduction. Energy Procedia 142: 501-506.

Kim, D., Sakimoto, K. K., Hong, D. and Yang, P. (2015). Artificial photosynthesis for sustainable fuel and chemical production Angew. Chem., Int. Ed. 54: 3259-3266.

Ku, Y., Ma, C. M. and Shen, Y. S. (2001). Decomposition of gaseous trichloroethylene in a photoreactor with TiO_2-coated nonwoven fiber textile. Appl. Catal., B 34: 181-190.

Kudo, A. and Miseki, Y. (2009). Heterogeneous photocatalyst materials for water splitting. Chem. Soc. Rev. 38: 253-278.

Leblebici, M. E., Stefanidis, G. D. and Van Gerven, T. (2015). Comparison of photocatalytic space-time yields of 12 reactor designs for wastewater treatment. Chem. Eng. Process. 97: 106-111.

Lee, J. C., Kim, M. S. and Kim, B. W. (2002). Removal of paraquat dissolved in a photoreactor with TiO_2 immobilized on the glass-tubes of UV lamps. Water Research 36: 1776-1782.

Lee, J. S., Lee, S. H., Kim, J. H. and Park, C. B. (2011). Artificial photosynthesis on a chip: Microfluidic cofactor regeneration and photoenzymatic synthesis under visible light. Lab Chip 11: 2309-2311.

Lee, S. H., Kim, J. H. and Park, C. B. (2013). Coupling photocatalysis and redox biocatalysis toward biocatalyzed artificial photosynthesis. Chem. - Eur. J. 19: 4392-4406.

Lee, S. H., Ryu, J., Nam, D. H. and Park, C. B. (2011). Photoenzymatic synthesis through sustainable NADH regeneration by SiO_2-supported quantum dots. Chem. Commun. 47: 4643-4645.

Lee, S. Y. and Park, S. J. (2013). TiO_2 photocatalyst for water treatment applications. J. Ind. Eng. Chem. 19: 1761-1769.

Lei, L., Wang, N., Zhang, X. M., Tai, Q., Tsai, D. P. and Chan, H. L. W. (2010). Optofluidic planar reactors for photocatalytic water treatment using solar energy. Biomicrofluidics 4: 043004.

Li, L., Chen, R., Liao, Q., Zhu, X., Wang, G. and Wang, D. (2014). High surface area optofluidic microreactor for redox mediated photocatalytic water splitting. Int. J. Hydrogen Energy. 39: 19270-19276.

Li, L., Chen, R., Zhu, X., Wang, H., Wang, Y., Liao, Q. and Wang, D. (2013). Optofluidic Microreactors with TiO_2-Coated Fiberglass. ACS Appl. Mater. Interfaces 5: 12548-12553.

Li, Y., Lin, B., Ge, L., Guo, H., Chen, X. and Lu, M. (2016). Real-time spectroscopic monitoring of photocatalytic activity promoted by graphene in a microfluidic reactor. Sci. Rep. 6: 1-9.

Lin, H. and Valsaraj, K. T. (2005). Development of an optical fiber monolith reactor for photocatalytic wastewater treatment. J. Appl. Electrochem. 35: 699-708.

Lin, S., Liu, Y., Hu, Z., Lu, W., Mak, C. H., Zeng, L., Zhao, J., Li, Y., Yan, F., Tsang, Y. H., et al. (2017). Tunable active edge sites in $PtSe_2$ films towards hydrogen evolution reaction. Nano Energy 42: 26-33.

Lin, S., Sun, S., Wang, K., Shen, K., Ma, B., Ren, Y. and Fan, X. (2018). Bioinspired design of alcohol dehydrogenase@nano TiO_2 microreactors for sustainable cycling of NAD^+/NADH coenzyme. Nanomaterials 8: 1-9.

Lin, Y., Yuan, G., Liu, R., Zhou, S., Sheehan, S. W. and Wang, D. (2011). Semiconductor nanostructure-based photoelectrochemical water splitting: A brief review. Chem. Phys. Lett. 507: 209-215.

Linic, S., Christopher, P. and Ingram, D. B. (2011). Plasmonic-metal nanostructures for efficient conversion of solar to chemical energy. Nat. Mater. 10: 911-921.

Liou, P. Y., Chen, S. C., Wu, J. C. S., Liu, D., MacKintosh, S., Maroto-Valer, M. and Linforth, R. (2011). Photocatalytic CO_2 reduction using an internally illuminated monolith photoreactor. Energy Environ. Sci. 4: 1487-1494.

Liu, C., Dasgupta, N. P. and Yang, P. (2014). Semiconductor nanowires for artificial photosynthesis. Chem. Mater. 26: 415-422.

Liu, J., Huang, J., Zhou, H. and Antonietti, M. (2014). Uniform Graphitic Carbon Nitride Nanorod for Efficient Photocatalytic Hydrogen Evolution and Sustained Photoenzymatic Catalysis. ACS Appl. Mater. Interfaces 6: 8434-8440.

Lu, D., Zhang, M., Zhang, Z., Li, Q., Wang, X. and Yang, J. (2014). Self-organized vanadium and nitrogen co-doped titania nanotube arrays with enhanced photocatalytic reduction of CO_2 into CH_4. Nanoscale Res. Lett. 9: 1-9.

Lu, H., Schmidt, M. A. and Jensen, K. F. (2001). Photochemical reactions and on-line UV detection in microfabricated reactors. Lab Chip 1: 22-28.

Ma, K., Yehezkeli, O., Park, E. and Cha, J. N. (2016). Enzyme Mediated Increase in Methanol Production from Photoelectrochemical Cells and CO_2. ACS Catal. 6: 6982-6986.

Ma, Y., Wang, X., Jia, Y., Chen, X., Han, H. and Li, C. (2014). Titanium dioxide-based nanomaterials for photocatalytic fuel generations. Chem. Rev. 114: 9987-10043.

Mak, X. Y., Laurino, P. and Seeberger, P. H. (2009). Asymmetric reactions in continuous flow. Beilstein J. Org. Chem. 5: 3-6.

Martin, M. V., Alfano, O. M. and Satuf, M. L. (2019). Cerium-doped TiO_2 thin films: Assessment of radiation absorption properties and photocatalytic reaction efficiencies in a microreactor. J. Environ. Chem. Eng. 7: 103478.

McCullagh, C., Skillen, N., Adams, M. and Robertson, P. K. J. (2011). Photocatalytic reactors for environmental remediation: A review. J. Chem. Technol. Biotechnol. 86: 1002-1017.

Mehendafe, S. S., Jacobi, A. M. and Shah, R. K. (2000). Fluid flow and heat transfer at micro- and meso-scales with application to heat exchanger design. Appl. Mech. Rev. 53: 175-193.

Mehendale, S. S., Jacobi, A. M. and Shah, R. K. (1999). Meso- and Micro-Scale Frontiers of Compact Heat Exchangers. 139-158.

Meng, Z., Zhang, X. and Qin, J. (2013). A high efficiency microfluidic-based photocatalytic microreactor using electrospun nanofibrous TiO_2 as a photocatalyst. Nanoscale 5: 4687-4690.

Midilli, A., Ay, M., Dincer, I. and Rosen, M. A. (2005). On hydrogen and hydrogen energy strategies I : Current status and needs. Renewable Sustainable Energy Rev. 9: 255-271.

Miller, T. E., Beneyton, T., Schwander, T., Diehl, C., Girault, M., McLean, R., Chotel, T., Claus, P., Cortina, N. S., Baret, J., et al. (2020). Light-powered CO_2 fixation in a chloroplast mimic with natural and synthetic parts. Science 368: 649-654.

Nagamine, S. (2020). Photocatalytic microreactor using TiO_2/Ti plates: Formation of TiO_2 nanostructure and separation of oxidation/reduction into different channels. Adv. Powder Technol. 31: 521-527.

Nagamine, S. and Inohara, K. (2018). Photocatalytic microreactor using anodized TiO_2 nanotube array. Adv. Powder Technol. 29: 3100-3106.

Nguyen, T. V. and Wu, J. C. S. (2008). Photoreduction of CO_2 in an optical-fiber photoreactor: Effects of metals addition and catalyst carrier. Appl. Catal., A 335: 112–120.

Oelgemoeller, M. (2012). Highlights of Photochemical Reactions in Microflow Reactors. Chem. Eng. Technol. 35: 1144-1152.

Oelgemöller, M. and Shvydkiv, O. (2011). Recent advances in microflow photochemistry. Molecules 16: 7522-7550.

Ola, O. and Maroto-Valer, M. M. (2015). Review of material design and reactor engineering on TiO_2

photocatalysis for CO_2 reduction. J. Photochem. Photobiol., C 24: 16-42.

Parmar, J., Jang, S., Soler, L., Kim, D. P. and Sánchez, S. (2015). Nano-photocatalysts in microfluidics, energy conversion and environmental applications. Lab Chip 15: 2352-2356.

Potti, P. R. and Srivastava, V. C. (2012). Comparative studies on structural, optical, and textural properties of combustion derived ZnO prepared using various fuels and their photocatalytic activity. Ind. Eng. Chem. Res. 51: 7948-7956.

Priyanka and Srivastava, V. C. (2013). Photocatalytic oxidation of dye bearing wastewater by iron doped zinc oxide. Ind. Eng. Chem. Res. 52: 17790-17799.

Psaltis, D., Quake, S. R. and Yang, C. (2006). Developing optofluidic technology through the fusion of microfluidics and optics. Nature 442: 381-386.

Qin, S., Xin, F., Liu, Y., Yin, X. and Ma, W. (2011). Photocatalytic reduction of CO_2 in methanol to methyl formate over CuO-TiO_2 composite catalysts. J. Colloid Interface Sci. 356: 257-261.

Russo, D. (2021). Kinetic modeling of advanced oxidation processes using microreactors: Challenges and opportunities for scale-up. Appl. Sci. 11: 1-19.

Ryu, J., Lee, S. H., Nam, D. H. and Park, C. B. (2011). Rational Design and Engineering of Quantum-Dot-Sensitized TiO_2 Nanotube Arrays for Artificial Photosynthesis. Adv. Mater. 23: 1883-1888.

De Sá, D. S., Marinkovic, B. A., Romani, E. C., Rosso, T. D., de Souza, R. O. M. A., Massi, A. and Pandoli, O (2016). Prototyping of meso- and microfluidic devices with embedded TiO_2 photocatalyst for photodegradation of an organic dye. J. Flow Chem. 6: 101-109.

De Sá, D. S., Vasconcelos, L. E., de Souza, J. R., Marinkovic, B. A., Del Rosso, T., Fulvio, D., Maza, D., Massi, A. and Pandoli, O. (2018). Intensification of photocatalytic degradation of organic dyes and phenol by scale-up and numbering-up of meso- and microfluidic TiO_2 reactors for wastewater treatment. J. Photochem. Photobiol. A 364: 59-75.

Sakimoto, K. K., Wong, A. B. and Yang, P. (2016). Self-photosensitization of nonphotosynthetic bacteria for solar-to-chemical production. Science 351: 74-77.

Sarkar, J. and Bhattacharyya, S. (2012). Application of graphene and graphene-based materials in clean energy-related devices Minghui. Arch. Thermodyn. 33: 23-40.

Schwander, T., Schada von Borzyskowski, L., Burgener, S., Cortina, N. S. and Erb, T. J. (2016). A synthetic pathway for the fixation of carbon dioxide in vitro. Science 354: 900-904.

Shafiq, I., Shafique, S., Akhter, P., Abbas, G., Qurashi, A. and Hussain, M. (2021). Efficient catalyst development for deep aerobic photocatalytic oxidative desulfurization: recent advances, confines, and outlooks. Catal. Rev.: Sci. Eng. 00: 1-46.

Shvydkiv, O., Yavorskyy, A., Tan, S. B., Nolan, K., Hoffmann, N., Youssef, A. and Oelgemöller, M. (2011). Microphotochemistry: A reactor comparison study using the photosensitized addition of isopropanol to furanones as a model reaction. Photochem. Photobiol. Sci. 10: 1399-1404.

Simms, R., Dubinsky, S., Yudin, A. and Kumacheva, E. (2009). A method for fabricating microfluidic electrochemical reactors. Lab Chip 9: 2395-2397.

Su, J. and Vayssieres, L. (2016). A Place in the Sun for Artificial Photosynthesis?. ACS Energy Lett. 1: 121-135.

Su, Y., Zhu, Y. and Fang, Q. (2013). A multifunctional microfluidic droplet-array chip for analysis by electrospray ionization mass spectrometry. Lab Chip 13: 1876.

Sun, M. and Fang, Q. (2010). High-throughput sample introduction for droplet-based screening with an on-chip integrated sampling probe and slotted-vial array. Lab Chip 10: 2864-2868.

Tan, C., Lo, S. J., Leduc, P. R. and Cheng, C. M. (2012). Frontiers of optofluidics in synthetic biology. Lab Chip 12: 3654-3665.

Tan, S. S., Zou, L. and Hu, E. (2006). Photocatalytic reduction of carbon dioxide into gaseous hydrocarbon using TiO_2 pellets. Catal. Today 115: 269-273.

Tao, Y., Wu, L., Zhao, X., Chen, X., Li, R., Chen, M., Zhang, D., Li, G. and Li, H. (2019). Strong Hollow Spherical La_2NiO_4 Photocatalytic Microreactor for Round-the-Clock Environmental Remediation. ACS Appl. Mater. Interfaces 11: 25967-25975.

Tian, Y., Zhou, Y., Zong, Y., Li, J., Yang, N., Zhang, M., Guo, Z. and Song, H. (2020). Construction of Functionally Compartmental Inorganic Photocatalyst-Enzyme System via Imitating Chloroplast for Efficient Photoreduction of CO2 to Formic Acid. ACS Appl. Mater. Interfaces 12: 34795-34805.

Tsuchiya, N., Kuwabara, K., Hidaka, A., Oda, K. and Katayama, K. (2012). Reaction kinetics of dye decomposition processes monitored inside a photocatalytic microreactor. Phys. Chem. Chem. Phys. 14: 4734-4741.

Ulmer, U., Dingle, T., Duchesne, P. N., Morris, R. H., Tavasoli, A., Wood, T. and Ozin, G. A. (2019). Fundamentals and applications of photocatalytic CO_2 methanation. Nat. Commun. 10: 1-12.

Van Gerven, T., Mul, G., Moulijn, J. and Stankiewicz, A. (2007). A review of intensification of

photocatalytic processes. Chem. Eng. Process. 46: 781-789.

Vesborg, P. C. K., In, S., Olsen, J. L., Henriksen, T. R., Abrams, B. L., Hou, Y., Kleiman-Shwarsctein, A., Hansen, O. and Chorkendorff, I. (2010). Quantitative measurements of photocatalytic CO-oxidation as a function of light intensity and wavelength over TiO_2 nanotube thin films in μ-reactors. J. Phys. Chem. C 114: 11162-11168.

Wang, N., Zhang, X., Chen, B., Song, W., Chan, N. Y. and Chan, H. L. W. (2012). Microfluidic photoelectrocatalytic reactors for water purification with an integrated visible-light source. Lab Chip 12: 3983-3990.

Wang, N., Zhang, X., Wang, Y., Yu, W. and Chan, H. L. W. (2014). Microfluidic reactors for photocatalytic water purification. Lab Chip 14: 1074-1082.

Wang, Q., Nakabayashi, M., Hisatomi, T., Sun, S., Akiyama, S., Wang, Z., Pan, Z., Xiao, X., Watanabe, T., Yamada, T., et al. (2019). Oxysulfide photocatalyst for visible-light-driven overall water splitting. Nat. Mater. 18: 827-832.

Wang, W. and Ku, Y. (2003). Photocatalytic degradation of gaseous benzene in air streams by using an optical fiber photoreactor. J. Photochem. Photobiol., A 159: 47-59.

Wang, Y., Vogel, A., Sachs, M., Sprick, R. S., Wilbraham, L., Moniz, S. J. A., Godin, R., Zwijnenburg, M. A., Durrant, J. R., Cooper, A. I., et al. (2019). Current understanding and challenges of solar-driven hydrogen generation using polymeric photocatalysts. Nat. Energy 4: 746-760.

Wang, Y., Wang, S. and Lou, X. W. (2019). Dispersed Nickel Cobalt Oxyphosphide Nanoparticles Confined in Multichannel Hollow Carbon Fibers for Photocatalytic CO_2 Reduction. Angew. Chem., Int. Ed. 58: 17236-17240.

Wang, Z. Y., Chou, H. C., Wu, J. C. S., Ping Tsai, D., Mul, G. and Engineering, C. (2010). CO_2 photoreduction using $NiO/InTaO_4$ in optical-fiber reactor for renewable energy. Appl. Catal., A 380: 172-177.

Whipple, D. T., Finke, E. C. and Kenis, P. J. A. (2010). Microfluidic reactor for the electrochemical reduction of carbon dioxide: The effect of pH. Electrochem. Solid-State Lett. 13: 109-111.

Whitesides, G. M. (2006). The origins and the future of microfluidics. Nature 442: 368-373.

Wu, H. Y., Nguyen, N. H., Bai, H., Chang, S. M. and Wu, J. C. S. (2015). Photocatalytic reduction of CO_2 using molybdenum-doped titanate nanotubes in a MEA solution. RSC Adv. 5: 63142-63151.

Wu, J. C. S., Lin, H. M. and Lai, C. L. (2005). Photo reduction of CO_2 to methanol using optical-fiber

photoreactor. Appl. Catal., A 296: 194-200.

Wu, J. C. S., Wu, T. H., Chu, T., Huang, H. and Tsai, D. (2008). Application of optical-fiber photoreactor for CO_2 photocatalytic reduction. Top. Catal. 47: 131-136.

Xie, F., Chen, R., Zhu, X., Liao, Q., Ye, D., Zhang, B., Yu, Y. and Li, J. (2019). CO_2 utilization: Direct power generation by a coupled system that integrates photocatalytic reduction of CO_2 with photocatalytic fuel cell. J. CO_2 Util. 32: 31-36.

Yang, D., Zhang, Y., Zhang, S., Cheng, Y., Wu, Y., Cai, Z., Wang, X., Shi, J. and Jiang, Z. (2019). Coordination between Electron Transfer and Molecule Diffusion through a Bioinspired Amorphous Titania Nanoshell for Photocatalytic Nicotinamide Cofactor Regeneration. ACS Catal. 9: 11492-11501.

Yu, G. and Wang, N. (2020). Gas-Liquid-Solid interface enhanced photocatalytic reaction in a microfluidic reactor for water treatment. Appl. Catal., A 591: 117410.

Yuan, K., Yang, L., Du, X. and Yang, Y. (2014). Performance analysis of photocatalytic CO_2 reduction in optical fiber monolith reactor with multiple inverse lights. Energy Convers. Manage. 81: 98-105.

Zeng, G., Qiu, J., Li, Z., Pavaskar, P. and Cronin, S. B. (2014). CO_2 reduction to methanol on TiO_2-passivated GaP photocatalysts. ACS Catal. 4: 3512-3516.

Zhang, H., Liu, H., Tian, Z., Lu, D., Yu, Y., Cestellos-Blanco, S., Sakimoto, K. K. and Yang, P. (2018). Bacteria photosensitized by intracellular gold nanoclusters for solar fuel production. Nat. Nanotechnol. 13: 900-905.

Zhang, H., Wang, J. J., Fan, J. and Fang, Q. (2013). Microfluidic chip-based analytical system for rapid screening of photocatalysts. Talanta 116: 946-950.

Zhang, S., Zhang, J., Sun, J. and Tang, Z. (2020). Capillary microphotoreactor packed with TiO_2-coated glass beads: An efficient tool for photocatalytic reaction. Chem. Eng. Process. 147: 107746.

Zhao, C., Xie, Y., Mao, Z., Zhao, Y., Rufo, J., Yang, S., Guo, F., Mai, J. D. and Huang, T. J. (2014). Theory and experiment on particle trapping and manipulation via optothermally generated bubbles. Lab Chip 14: 384-391.

Zhao, D., He, Z., Wang, G., Wang, H., Zhang, Q. and Li, Y. (2016). A novel efficient ZnO/Zn(OH)F nanofiber arrays-based versatile microfluidic system for the applications of photocatalysis and histidine-rich protein separation. Sens. Actuators, B 229: 281-287.

Zhao, Y., Liu, H., Wu, C., Zhang, Z., Pan, Q., Hu, F., Wang, R., Li, P., Huang, X. and Li, Z. (2019).

Fully Conjugated Two-Dimensional sp^2-Carbon Covalent Organic Frameworks as Artificial Photosystem I with High Efficiency. Angew. Chem., Int. Ed. 58: 5376-5381.

Zhou, N., López-Puente, V., Wang, Q., Polavarapu, L., Pastoriza-Santos, I. and Xu, Q-H. (2015). Plasmon-enhanced light harvesting: Applications in enhanced photocatalysis, photodynamic therapy and photovoltaics. RSC Adv. 5: 29076-29097.

Zhu, Y., Huang, Z., Chen, Q., Wu, Q., Huang, X., So, P. K., Shao, L., Yao, Z., Jia, Y., Li, Z., at al. (2019). Continuous artificial synthesis of glucose precursor using enzyme-immobilized microfluidic reactors. Nat. Commun. 10: 1-9.

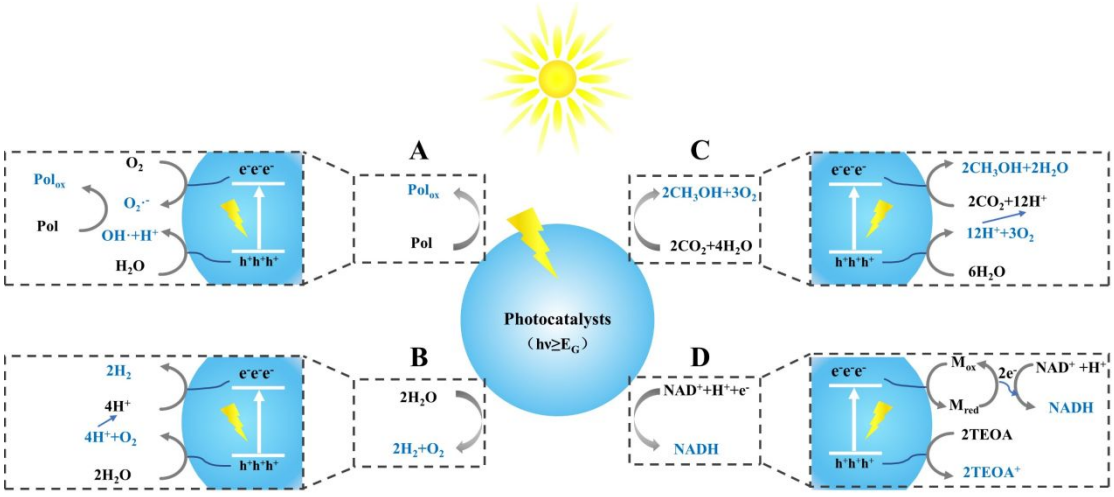

Fig. 1 Mechanism of photocatalytic, (A) water purification. "Pol" refers to pollutants, while "Pol_{ox}" refers to the oxidation products of pollutants; (B) water splitting; (C) CO_2 fixation (take methanol as an example) and (D) synthesis of coenzyme. TEOA in the picture is an electron sacrificial agent, used to consume photo-generated holes, M_{ox} and M_{red} refer to the oxidation state and reduction state of the electron transfer medium(M).

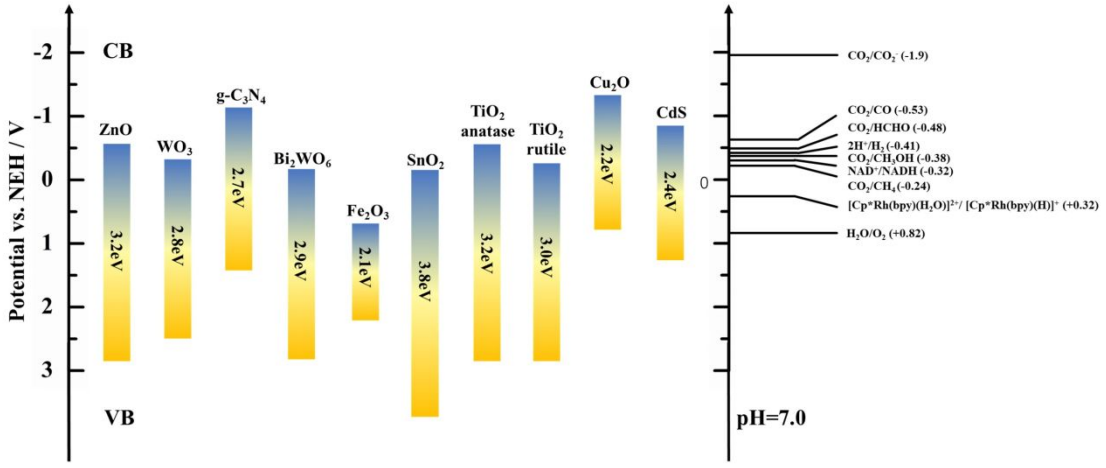

Fig. 2 The band gap of some photocatalysts and the redox potential of different chemical species at pH of 7.0 (Ola and Maroto-Valer, 2015).

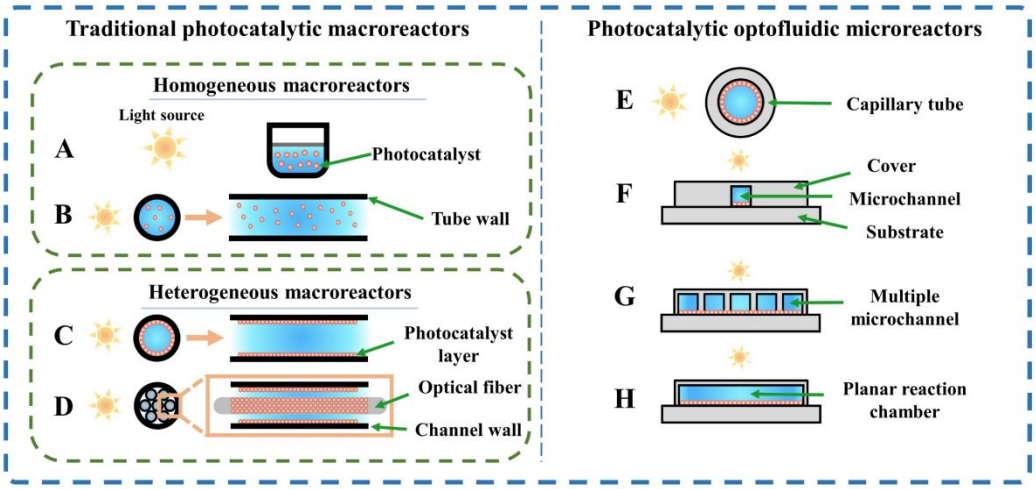

Fig. 3 Schematic of photocatalytic reactors. (A) Schematic of batch macroreactors (with the volume ranges from several cubic centimeters to hundreds of cubic centimeters); (B) Schematic of flow mode macroreactors (D_h > 1 mm); (C) Schematic of wall-coated macroreactors (D_h > 1 mm); (D) Schematic of honeycomb optical fiber macroreactors (D_h > 1 mm); (E) Schematic of capillary tube microreactor; (F) Schematic of single-microchannel reactor; (G) Schematic of multi-microchannel reactor; (H) Schematic of planar microreactor. The D_h of photocatalytic optofluidic microreactor is less than 1 mm.

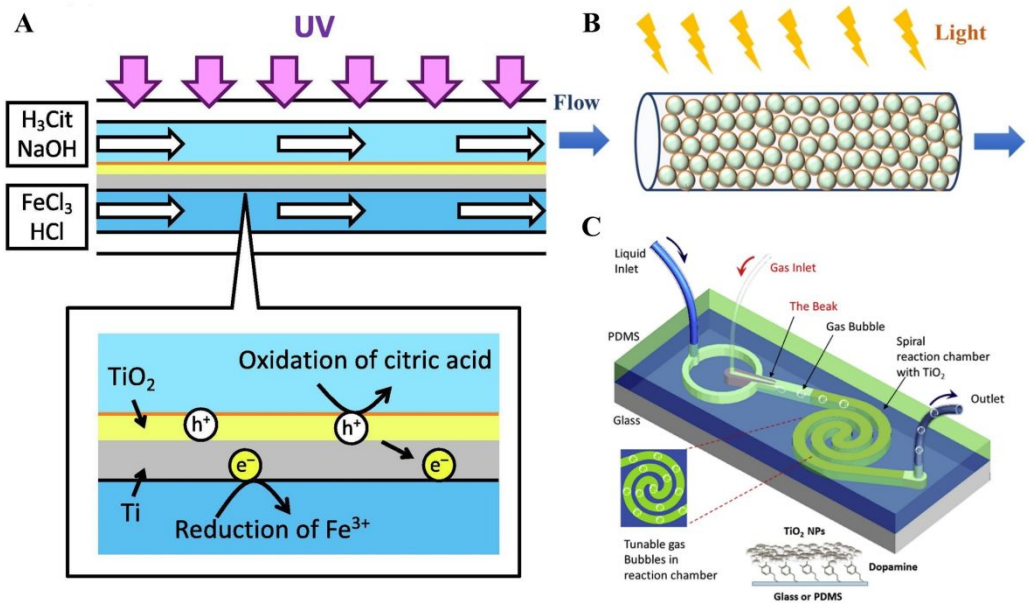

Fig. 4 (A) Schematic of the developed photocatalytic microreactor with separated oxidation and reduction channels (Nagamine 2020). Copyright © 2019 The Society of Powder Technology Japan. (B) Schematic of the capillary microreactor packed with TiO_2-coated glass beads (Zhang et al. 2020). Copyright © 2020 Elsevier B. V. (C) Device design of the triphasic photocatalytic microreactor (Yu and Wang 2020). Copyright © 2019 Elsevier B. V.

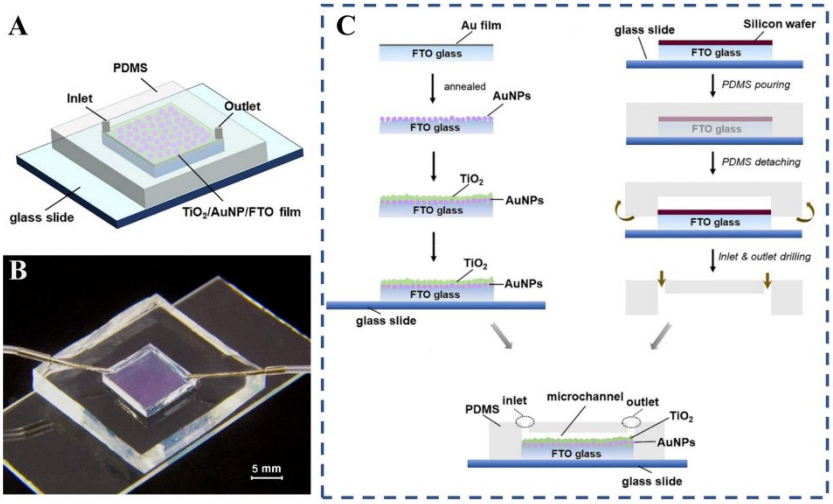

Fig. 5 TiO_2/AuNP microreactor. (A) 3D diagram of the TiO_2/AuNP microreactor (Jia et al. 2019). Copyright © 2019 MDPI. (B) Photo of the TiO_2/AuNP microreactor (Jia et al. 2019). Copyright © 2019 MDPI. (C) Fabrication and integration of the microreactor. On the left side of the picture is fabrication process of the TiO_2/AuNP film; On the right side of the picture is non-photolithographic manual molding of the polydimethylsiloxane (PDMS) cover; And at the bottom of the picture is cross-sectional view of the microreactor after the PDMS cover is bonded on the TiO_2/AuNP film (Jia et al. 2019). Copyright © 2019 MDPI.

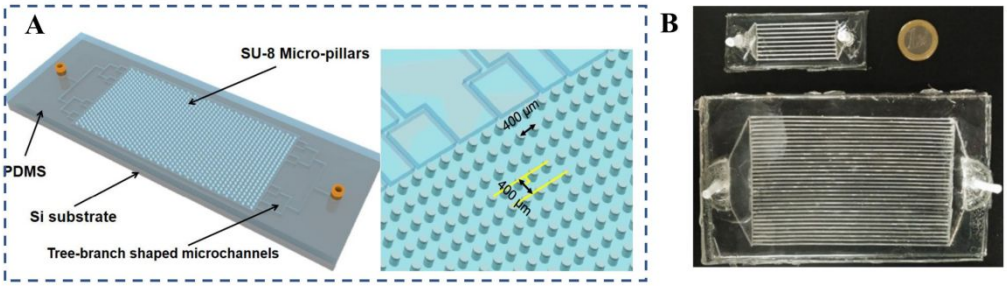

Fig. 6 (A) Schematic of the optofluidic microreactor with micropillar structure and cross section of the staggered micro-pillars in the reaction chamber (Li et al. 2014). Copyright © 2014 Hydrogen Energy Publications, LLC. (B) Photographs of two size of silicone microreactors. The small microreactor and the large microreactor showed a very similar result in terms of hydrogen production (Castedo et al. 2018). Copyright © 2018 Elsevier Ltd.

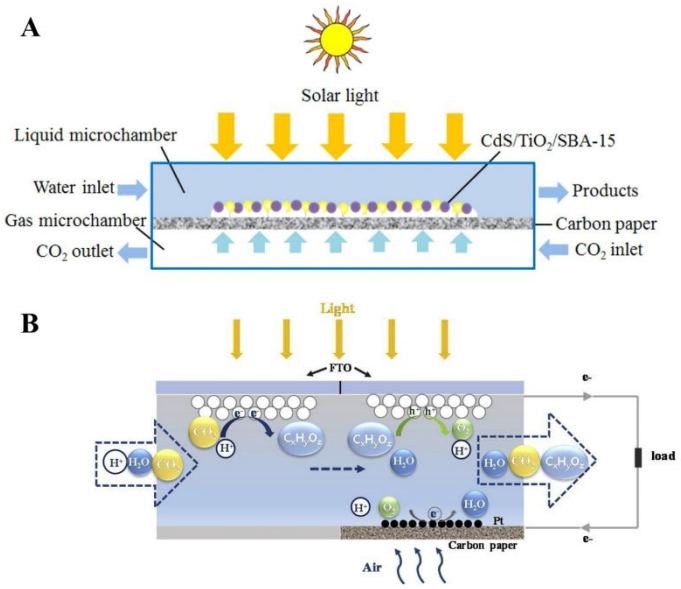

Fig. 7 (A) Schematic of the optofluidic membrane microreactor (Chen et al. 2017). Copyright © 2017 Elsevier B.V (B) Working principle of the coupled system that integrates photocatalytic reduction of CO_2 with photocatalytic fuel cell (Xie et al. 2019). Copyright © 2019 Elsevier Ltd.

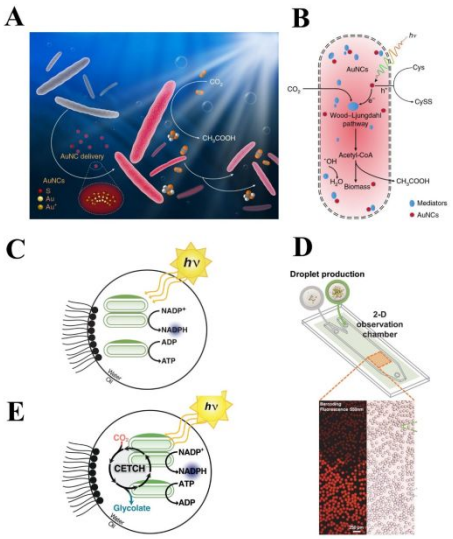

Fig. 8 (A) Schematic diagram of the *M. thermoacetica*/AuNC hybrid system (Zhang et al. 2018). Copyright © 2018 Springer Nature. (B) The electrons generated from intracellular AuNCs under illumination are used by enzymatic mediators inside the cytoplasm and are finally passed on to the Wood-Ljungdahl pathway (Zhang et al. 2018). Copyright © 2018 Springer Nature. (C) Scheme of the thylakoid membrane–based energy module (TEM) system encapsulated in microdroplets. Light triggers TEM activity to produce NADPH and ATP (Miller et al. 2020). Copyright © 2020 The American Association for the Advancement of Science. (D) Schematic of the reactor used for time and spatial control of metabolic activity in droplets, and the spatial pattern of two different droplets in the observation chamber (Miller et al. 2020). Copyright © 2020 The American Association for the Advancement of Science. (E) Scheme of the CETCH coupled to TEM operating inside microdroplets (Miller et al. 2020). Copyright © 2020 The American Association for the Advancement of Science.

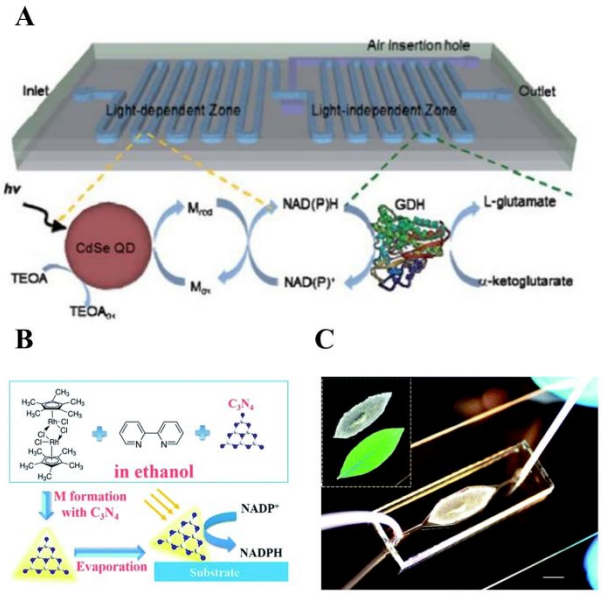

Fig. 9 (A) Design of microreactor, in which the cofactor regeneration takes place in the light-dependent reaction zone and the enzymatic synthesis in the light-independent zone (J. S. Lee et al. 2011). Copyright © 2011 Royal Society of Chemistry. (B) One-step fabrication process of the immobilized artificial Photosystem I (IAPSI) (Huang, Liu, et al. 2016). Copyright © 2016 The Royal Society of Chemistry. (C) Photograph of the as-fabricated IAPSI microreactor, in which the inset presents the leaf-like shape of photocatalysts with electron mediators (Huang, Liu, et al. 2016). Copyright © 2016 The Royal Society of Chemistry.

Table 1 Photocatalytic optofluidic microreactors used for photocatalytic water purification, water splitting, CO_2 fixation and coenzyme regeneration.

Reaction type	Catalyst	Light source	Model chemicals	Catalytic efficiency	Standard catalytic efficiency
Water purification	ZnO NWs	UV lamp (365 nm, 4500 mW cm^{-2})	Volatile organic compounds (2000 μg mL^{-1})	95% (5 s) (Azzouz et al. 2018)	2.28×10^4 μg mL^{-1} min^{-1}
	TiO_2	Xe-lamp (107 mW cm^{-2})	Methylene blue (3.13×10^{-5} mol L^{-1})	96% (20 s) (Zhang et al. 2020)	~28.83 μg mL^{-1} min^{-1}
	TiO_2/AuNP	Xe-lamp (λ＞420 nm, 300 mW cm^{-2})	Methylene blue (5×10^{-5} mol L^{-1})	58% (12.5 min) (Jia et al. 2019)	~0.74 μg mL^{-1} min^{-1}
	Ce-TiO_2	Solar simulator (300-500 nm, 3.55 mW cm^{-2})	17-α-Ethinylestradiol (9 mg L^{-1})	86% (14 min) (Martin et al. 2019)	~0.55 μg mL^{-1} min^{-1}
Water splitting	CdS	Hg lamp (450W, λ＞380 nm)	H_2	5.21 mmol h^{-1} g^{-1} (An et al. 2019)	5.21 mmol g_{cat}^{-1} h^{-1}
	Au/TiO_2	LED (365±2 nm, 1.5 mW cm^{-2})	H_2	0.99 ± 0.024 mmol h^{-1} g^{-1} (Castedo et al. 2018)	0.99 ± 0.024 mmol g_{cat}^{-1} h^{-1}
CO_2 fixation	Cu_2^+-TiO_2	UV-LED (365 nm, 15 mW cm^{-2})	Methanol /Ethanol	36.18 μmol g_{cat}^{-1} h^{-1} /79.13 μmol g_{cat}^{-1} h^{-1} (Cheng et al. 2017)	0.03618 mmol g_{cat}^{-1} h^{-1} /0.07913 mmol g_{cat}^{-1} h^{-1}
	TiO_2/carbon paper composite membrane	LED (365 nm, 8 mW cm^{-2})	Methanol	111.0 μmol $g_{cat}^{-1}h^{-1}$ (Cheng et al. 2016)	0.111 mmol $g_{cat}^{-1}h^{-1}$
	CdS/20 wt% TiO_2/SBA-15	Xe-lamp (400-540nm, 100 mW cm^{-2})	Methanol	1022 μmol g_{cat}^{-1} h^{-1} (Chen et al. 2017)	1.022 mmol $g_{cat}^{-1}h^{-1}$

Regeneration of coenzyme	CdSe	Xe-lamp (λ> 420 nm, 62 mW cm^{-2})	NADH (1 mmol L^{-1})	27% (60 min) (J. S. Lee et al. 2011)	0.27 mmol L^{-1} h^{-1}
	Few-layer g-C_3N_4	Xe-lamp (λ> 420 nm)	NADH (1 mmol L^{-1})	56% (30 min) (Huang et al. 2016)	1.12 mmol L^{-1} h^{-1}
	Carbon nitride nanorods (CNR)	LED lamp	NADH (1 mmol L^{-1})	72% (60 min) (Liu et al. 2014)	0.72 mmol L^{-1} h^{-1}

*Definition of different standard catalytic efficiency unit: (1) Water purification: Based on the degradation rate, reaction time and initial concentration., the pollutant degradation efficiency units were converted to [μg mL^{-1} min^{-1}]; (2) Water splitting and CO_2 fixation: the parameters included in the photocatalytic efficiency units are consistent, e.g., in the units [mmol h^{-1} g^{-1}] and [μmol g_{cat}^{-1} h^{-1}], both [g] and [g_{cat}] denote the mass of the catalyst, h denotes hours, and both [mmol] and [μmol] denote the yield of the product. To avoid confusion, the standard catalytic efficiency is unified into [mmol g_{cat}^{-1} h^{-1}]; (3) Synthesis of coenzyme: The coenzyme regeneration efficiency units were converted to [mmol L^{-1} h^{-1}] according to the regeneration rate, reaction time and initial concentration.

Table 2 Type of traditional photocatalytic macroreactors used for photocatalysis.

Type of macroreactor	Catalyst	Light source	Model chemicals	Catalytic efficiency	Standard catalytic efficiency	Dimensions (cm^3)
Homogeneous photoreactors	Mo-TNTs	UVA lamp (365 nm, 0.063 mW cm^{-2})	CH_4/CO	0.087 μmol g_{cat}^{-1} h^{-1} /1.735 μmol g_{cat}^{-1} h^{-1} (Wu et al. 2015)	8.7×10^{-5} mmol g_{cat}^{-1} h^{-1} /1.735×10^{-3} mmol g_{cat}^{-1} h^{-1} (Wu et al. 2015)	300
Heterogeneous photoreactors (Wall-coated)	TiO_2 pellets	UVC lamp (253.7 nm)	CH_4	200 ppm (48 h) (Tan et al. 2006)	~2.02×10^{-6} mmol g_{cat}^{-1} h^{-1}	1088.95
	TiO_2	Hg lamp (6 W)	Paraquat (100 mg L^{-1})	99% (12 h) (Lee et al. 2002)	0.1375 μg mL^{-1} min^{-1}	1000
	TiO_2 pellets	Hg UV tubes (365 nm, 1.1 mW cm^{-2})	Phenol (0.038 mmol L^{-1})	86% (6 h) (Dionysiou et al. 2000)	~8.47×10^{-3} μg mL^{-1} min^{-1}	5000
Heterogeneous photoreactors (Optical fiber)	Cu-Fe/TiO_2	Hg lamp (320-500 nm, 225 mW cm^{-2})	Methane/ Ethylene	0.91 μmol g_{cat}^{-1} h^{-1}/ 0.58 μmol g_{cat}^{-1} h^{-1} (Nguyen and Wu 2008)	9.1×10^{-4} mmol g_{cat}^{-1} h^{-1}/ 5.8×10^{-4} mmol g_{cat}^{-1} h^{-}	216
	Cu/TiO_2	Hg lamp (365 nm, 16000 mW cm^{-2})	Methanol	0.45 μmol g_{cat}^{-1} h^{-1} (Wu et al. 2005))	4.5×10^{-4} mmol g_{cat}^{-1} h^{-1}	128.6
	TiO_2	UV lamp (365 nm, 40 W)	Gaseous benzene (20 ppmv)	80% (4 h) (Wang and Ku 2003)	---	195

Table 3. Comparison of traditional photocatalytic macroreactors and photocatalytic optofluidic microreactors.

Index	Traditional photocatalytic macroreactor	Photocatalytic optofluidic microreactor
Surface-to-volume ratio	Low specific surface area, mostly <3000 m^2 m^{-3} (Van Gerven et al. 2007)	High specific surface area, 10000-300000 m^2 m^{-3} (Lu et al. 2001; Lei et al. 2010; Mak et al. 2009; Meng et al. 2013; Wang et al. 2014; Vesborg et al. 2010)
Molecular diffusion length	Millimeters or centimeters (Lin and Valsaraj 2005; Van Gerven et al. 2007)	Microns (Huang et al. 2018; Wang et al. 2014)
Irradiation	Not uniform (Oelgemoeller 2012)	Uniform irradiation due to immobilized photocatalyst (Chong et al. 2010)
Reaction time	Usually in the range of 4 to 48 hours (Oelgemoeller 2012)	Most are less than an hour, some even less than a minute (Lei et al. 2010; Meng et al. 2013; Wang et al. 2012)
Stability of the photocatalysts	About 10 runs of reactions (Chen et al. 2013; McCullagh et al. 2011; Wu et al. 2008)	Several hundred runs of reactions (Wang et al. 2012)
Control of fluids	Extensive control	Fine control by precision syringe pump (Elvira et al. 2013; Erickson et al. 2011; Psaltis et al. 2006)

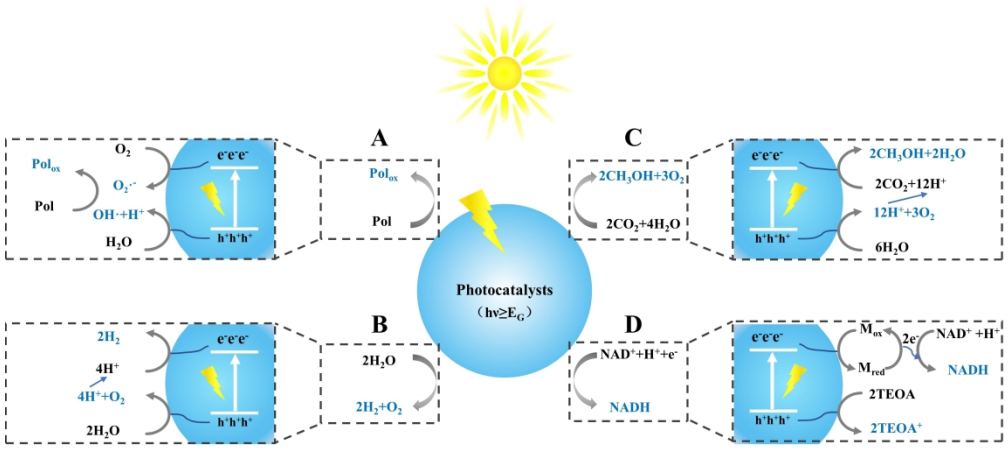

Fig. 1 Mechanism of photocatalytic, (A) water purification. "Pol" refers to pollutants, while "Polox" refers to the oxidation products of pollutants; (B) water splitting; (C) CO2 fixation (take methanol as an example) and (D) synthesis of coenzyme. TEOA in the picture is an electron sacrificial agent, used to consume photo-generated holes, Mox and Mred refer to the oxidation state and reduction state of the electron transfer medium(M).

338x190mm (300 x 300 DPI)

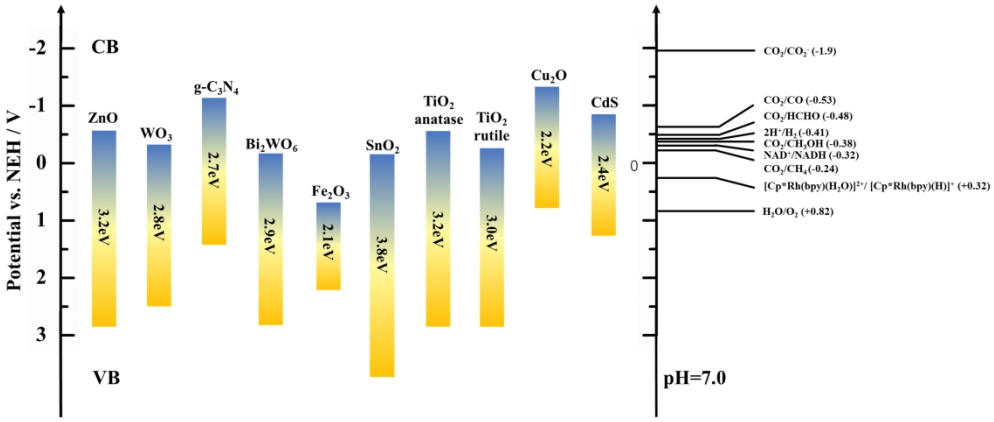

Fig. 2 The band gap of some photocatalysts and the redox potential of different chemical species at pH of 7.0 (Ola and Maroto-Valer, 2015).

338x190mm (300 x 300 DPI)

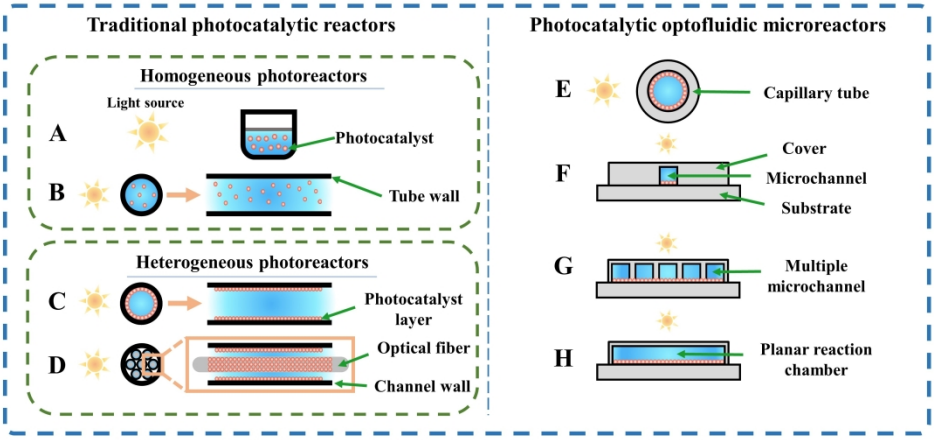

Fig. 3 Schematic of photocatalytic reactors. (A) and (B) Schematic of homogeneous photoreactors; (C) Schematic of wall-coated photoreactors; (D) Schematic of honeycomb optical fiber reactors; (E) Schematic of capillary tube microreactor (inner diameter: ≤ 1 mm); (F) Schematic of single-microchannel reactor; (G) Schematic of multi-microchannel reactor; (H) Schematic of planar microreactor.

338x190mm (300 x 300 DPI)

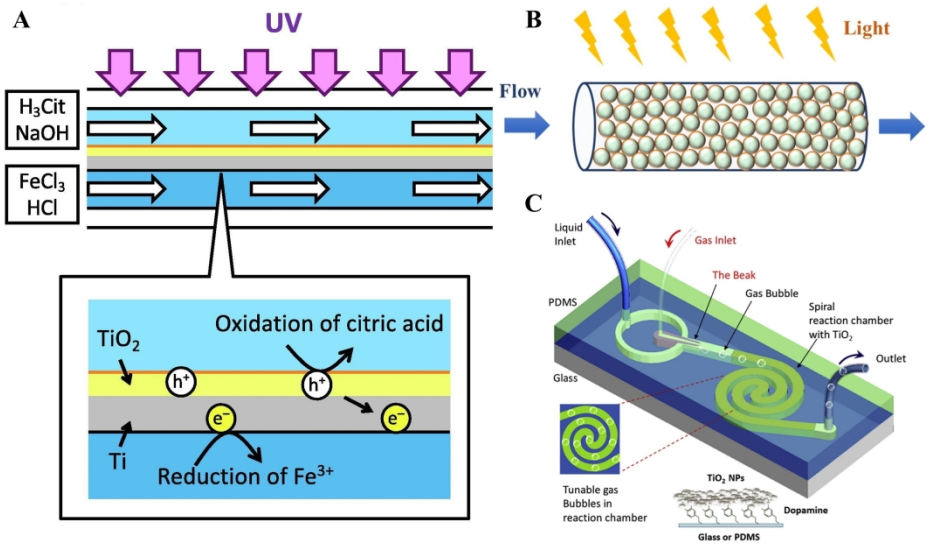

Fig. 4 (A) Schematic of the developed photocatalytic microreactor with separated oxidation and reduction channels (Nagamine 2020). Copyright © 2019 The Society of Powder Technology Japan. (B) Schematic of the capillary microreactor packed with TiO2-coated glass beads (Zhang et al. 2020). Copyright © 2020 Elsevier B. V. (C) Device design of the triphasic photocatalytic microreactor (Yu and Wang 2020). Copyright © 2019 Elsevier B. V.

338x190mm (300 x 300 DPI)

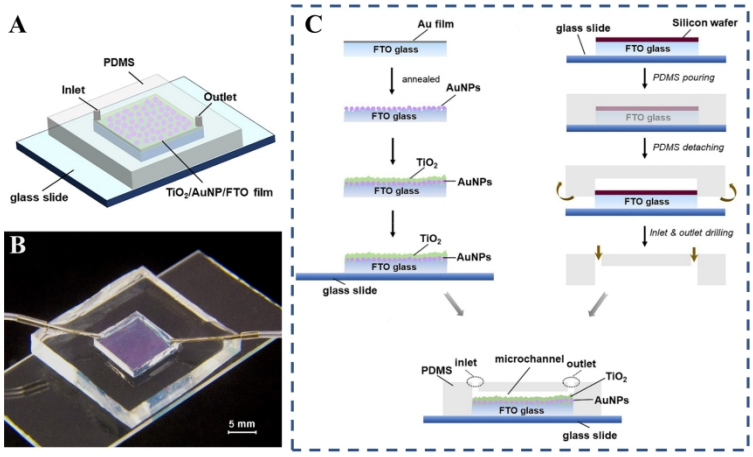

Fig. 5 TiO2/AuNP microreactor. (A) 3D diagram of the TiO2/AuNP microreactor (Jia et al. 2019). Copyright © 2019 MDPI. (B) Photo of the TiO2/AuNP microreactor (Jia et al. 2019). Copyright © 2019 MDPI. (C) Fabrication and integration of the microreactor. On the left side of the picture is fabrication process of the TiO2/AuNP film; On the right side of the picture is non-photolithographic manual molding of the polydimethylsiloxane (PDMS) cover; And at the bottom of the picture is cross-sectional view of the microreactor after the PDMS cover is bonded on the TiO2/AuNP film (Jia et al. 2019). Copyright © 2019 MDPI.

338x190mm (300 x 300 DPI)

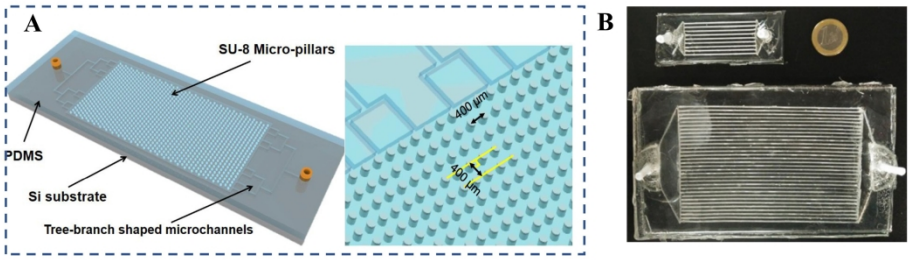

Fig. 6 (A) Schematic of the optofluidic microreactor with micropillar structure and cross section of the staggered micro-pillars in the reaction chamber (Li et al. 2014). Copyright © 2014 Hydrogen Energy Publications, LLC. (B) Photographs of two size of silicone microreactors. The small microreactor and the large microreactor showed a very similar result in terms of hydrogen production (Castedo et al. 2018). Copyright © 2018 Elsevier Ltd.

338x190mm (300 x 300 DPI)

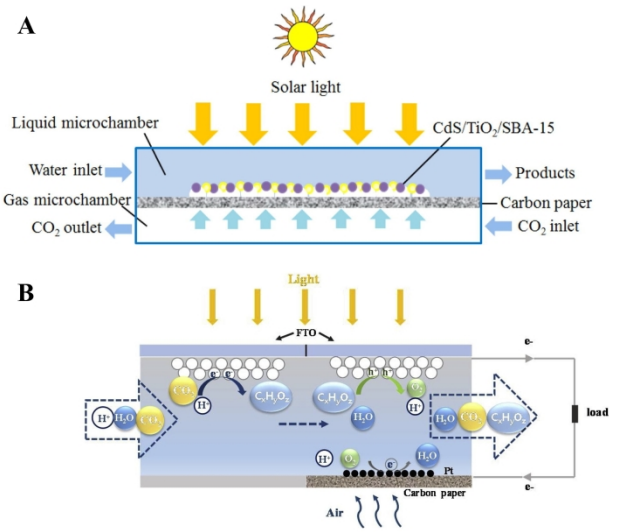

Fig. 7 (A) Schematic of the optofluidic membrane microreactor (Chen et al. 2017). Copyright © 2017 Elsevier B.V (B) Working principle of the coupled system that integrates photocatalytic reduction of CO2 with photocatalytic fuel cell (Xie et al. 2019). Copyright © 2019 Elsevier Ltd.

338x190mm (300 x 300 DPI)

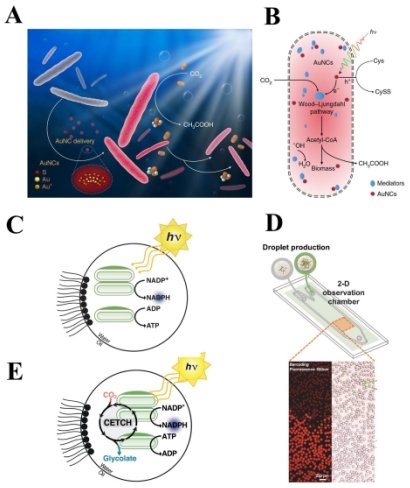

Fig. 8 (A) Schematic diagram of the M. thermoacetica/AuNC hybrid system (Zhang et al. 2018). Copyright © 2018 Springer Nature. (B) The electrons generated from intracellular AuNCs under illumination are used by enzymatic mediators inside the cytoplasm and are finally passed on to the Wood-Ljungdahl pathway (Zhang et al. 2018). Copyright © 2018 Springer Nature. (C) Scheme of the thylakoid membrane–based energy module (TEM) system encapsulated in microdroplets. Light triggers TEM activity to produce NADPH and ATP (Miller et al. 2020). Copyright © 2020 The American Association for the Advancement of Science. (D) Schematic of the reactor used for time and spatial control of metabolic activity in droplets, and the spatial pattern of two different droplets in the observation chamber (Miller et al. 2020). Copyright © 2020 The American Association for the Advancement of Science. (E) Scheme of the CETCH coupled to TEM operating inside microdroplets (Miller et al. 2020). Copyright © 2020 The American Association for the Advancement of Science.

338x190mm (300 x 300 DPI)

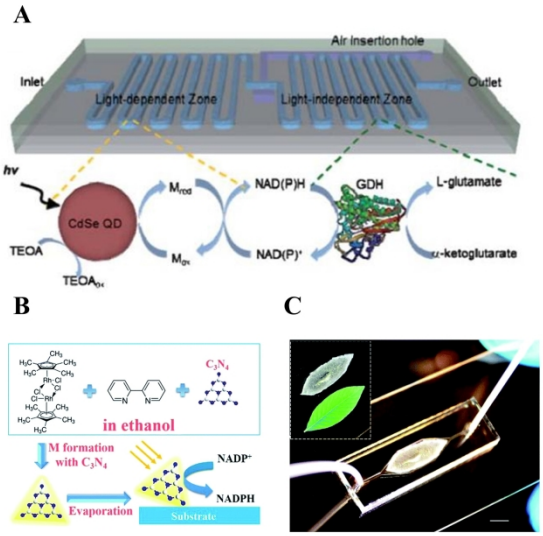

Fig. 9 (A) Design of microreactor, in which the cofactor regeneration takes place in the light-dependent reaction zone and the enzymatic synthesis in the light-independent zone (J. S. Lee et al. 2011). Copyright © 2011 Royal Society of Chemistry. (B) One-step fabrication process of the immobilized artificial Photosystem I (IAPSI) (Huang, Liu, et al. 2016). Copyright © 2016 The Royal Society of Chemistry. (C) Photograph of the as-fabricated IAPSI microreactor, in which the inset presents the leaf-like shape of photocatalysts with electron mediators (Huang, Liu, et al. 2016). Copyright © 2016 The Royal Society of Chemistry.

338x190mm (300 x 300 DPI)